


## Article

# Elemental and Mineral Composition of the Barents Sea Recent and Late Pleistocene–Holocene Sediments: A Correlation with Environmental Conditions

Liudmila L. Demina <sup>1,\*</sup> , Olga Dara <sup>1</sup>, Ramiz Aliev <sup>2</sup>, Tatiana Alekseeva <sup>1</sup>, Dmitry Budko <sup>1</sup>, Ekaterina Novichkova <sup>1</sup>, Nadezhda Politova <sup>1</sup>, Aleksandra Solomatina <sup>1</sup> and Anton Bulokhov <sup>1</sup>

<sup>1</sup> Shirshov Institute of Oceanology, Russian Academy of Sciences, 36 Nakhimovsky Prospect, 117997 Moscow, Russia; olgadara@mail.ru (O.D.); tania@blackout.ru (T.A.); dmitry.b-1990@yandex.ru (D.B.); enovichkova@mail.ru (E.N.); politova@ocean.ru (N.P.); balckmaple@yandex.ru (A.S.); vincentrmsne@rambler.ru (A.B.)

<sup>2</sup> Department of Chemistry, Lomonosov Moscow State University, GSP-1, Leninskie Gory, 1, 119991 Moscow, Russia; ramiz.aliev@gmail.com

\* Correspondence: l\_demina@mail.ru

Received: 7 June 2020; Accepted: 28 June 2020; Published: 30 June 2020



**Abstract:** A comprehensive examination of the elemental (including radionuclides and heavy metals), mineral, and grain-size composition of sediments from different areas of the Barents Sea was performed. Sediment cores were sampled in the Central Deep, Cambridge Strait (Franz Josef Land Archipelago), Russkaya Gavan' Bay (Novaya Zemlya Archipelago), and Bear Island Trough. We aim to evaluate how the modern and more ancient environmental conditions are reflected in the elemental and mineral composition, as well as to test indicative elemental ratios. The applied methods include elemental analysis using gamma-ray spectroscopy, X-ray fluorescence (XRF), Inductively Coupled Plasma-Mass Spectrometry (ICP-MS), and X-Ray Diffractometry XRD analysis of minerals. Difference in sedimentation rates, grain-size composition, and sources of material, are reflected in downcore variation of Si/Al, Mn/Fe, P/Al, Ti/K, and quartz-feldspar ratios. At boundary Early Holocene/Late Deglaciation, intensive bottom currents from the West-Southern shelf areas contributed to increase of Si/Al and Zr/Ca ratios. Distinct growth of the Si/Fe ratio within the sediments deposited over Late Pleistocene to Mid Holocene may be caused by increased contents of the coarse sand material, as well as by abundant fluxes of clay-mineral-loaded glacial meltwater during the main deglaciation phase. The Mn/Fe ratio used as redox proxy, displayed peaks at different depths related to oxygen concentration growth in bottom water.

**Keywords:** Barents Sea; sediment cores; radionuclides; grain-size and mineral composition; major and trace elements; proxies

## 1. Introduction

The Barents Sea is one of the key areas for investigating the post-glacial climate change. There, the penetration of relatively warm North Atlantic water into the Arctic is almost completed, while an interaction of the Barents Sea and the Arctic waters takes place. During the late Pleistocene–Holocene (18–14.5 cal ka Before Present BP), penetration of the relatively warm Atlantic waters through the Fram Strait and eastward along the margin of the Scandinavian–Barents Ice Sheet into the Arctic Ocean contributed to the ice sheets' melting and meant a start of deglaciation of the Western Eurasian shelf [1,2]. In the early stage of deglaciation, relatively coarse-grained (sand-silt-pelite with gravel and pebbles) glacial-marine sediments were accumulated. Late deglaciation was characterized by the processes of near-bottom transport and resuspension with the formation of laminated deposits

by nepheloid flows, as well as of turbidites composed of mostly fine-dispersed terrigenous material formed by meltwater of the retreating glaciers. During the Holocene, normal marine sedimentation was developed, wherein, several stages have been identified based on lithological and micropaleontological (foraminifera) data, reflecting changes in the intensity of Atlantic waters entering the Barents Sea [3,4].

Holocene sediments, deposited at average sedimentation rate less than 10 cm/1000 years, when comparing to deglacial sediments, are characterized by elevated and variable contents of organic carbon, Cu, Ni, V, Sr, Cr, Mn, V, and Ti, which might be attributed to change in sources and sedimentation environment [5]. Glacial sediments were formed in a colder climate, when the major role in the transport of elements to sediments belonged to the products of glacial activity, such as the Upper Pleistocene clayey-silt with a noticeable content of sand. Glacial deposits accumulated earlier than 10 cal. ka BP, are characterized by minimal variability of chemical elements due to the only aeolian source of sedimentary material at that time [5].

In the sediment sequences, various parameters of paleoenvironment are recorded, among them, there are physical proxies (e.g. grain-size composition, magnetic sustainability), organic and inorganic geochemical proxies, and biological proxies (e.g. microfossils abundance) [6]. Elemental composition may be used as potential proxies of changes in terrestrial runoff, paleoproductivity of water mass, and source of sedimentary material [7]. Based on elemental, isotope, and mineral indicators, important paleo-environmental characteristics, including dramatic climate shifts in the Northern Hemisphere, were reconstructed. In the late Quaternary sediment cores of the Arctic Ocean, the Si/Al, Fe/Ca, Ti/Al, and Zr/Al ratios were applied to estimate the variability of clastic components; a growth of these ratios during the deglacial periods characterizes a predominance of physical weathering over the chemical one [7–9]. Increases in sand percentages and the quartz/plagioclase ratio are concurrent with decreasing log (Ti/K) ratios, suggesting major changes in the provenance and transport mechanism of the sediment. All three parameters point to a continental crust derived ice-rafted origin of the sediment [10]. The proportion of clay minerals (kaolinite and illite) characterizes the pelitic and coarse silt/sand fractions in the sediments of Mendeleev Ridge [11]. The feeding provinces of the Lena, Yenisei and Ob rivers' catchment are identified by the composition of clay and heavy minerals, as well as by changes in the elemental indicative ratios Ti/Al, Cr/Al, and Ni/Al in the sediments of the shelf of the Kara and the Laptev Seas [12]. To identify sources of the sedimentary material, a combination of different isotope methods is used. Based on isotope ratios of  $^{207}\text{Pb}/^{206}\text{Pb}$ ,  $^{87}\text{Sr}/^{86}\text{Sr}$ , and  $\epsilon\text{Nd}$ , it was shown that modern sedimentation in the central Barents Sea was primary controlled by contribution of fine-grained sedimentary materials from the weathered rocks of the Northern European continental margin, transported by the North Cape Current, while the ice-rafted material was supplied with Transpolar Drift [13].

The Barents Sea, whose area amounts to only about 7% of total area of all Arctic seas, contains the main part of the Arctic marine biological resources [14]. Possibly due to it, the first geochemical investigation was related to examination of biogenic components (TOC,  $\text{CaCO}_3$ ,  $\text{bioSiO}_2$ ) [15–17]. Subsequently, distribution patterns of these components, as well as of major and some trace metals, were studied in different types of the Barents Sea sediments [5,18,19]. The Barents Sea, being a key segment of the Northern marine route and as a region, rich in mineral resources (Shtockman gas-condensate field, etc.), is an important basin to study various contaminants. Detailed examination of pollutants (oil hydrocarbons, polycyclic aromatic hydrocarbons, phenols, organic chlorine compounds, heavy metals, and radionuclides), as well as their sources and distribution pattern, were studied in [20]. A large data set on their distribution in surface sediments collected from the entire sea area over the period of 1998–2015 was analyzed to assess a degree of heavy metal contamination in the Barents Sea [21].

Thus, the Barents Seas is a suitable basin to study peculiarities of elemental geochemistry and mineral composition under the deglaciation, postglacial, and modern environmental conditions in the shallow areas of the Arctic Ocean. Geochemical characteristics of marine sediments, particularly of potentially toxic heavy metals, are of interest to evaluate and/or predict the risks for the environment.

Taking the significant research results mentioned above into account, it should be noticed that less attention was paid to elemental geochemical and/or mineral indicators of the modern and paleo-sedimentation environment of the Barents Sea. Geochemical fractions (chemical element speciation) serve as an important tool to quantify different processes of elements' accumulation in sediments and assess the geochemical cycles of heavy metals in the different marine basins [22–29].

In this work, based on new comprehensive data on basic lithological, elemental (including the radionuclides and heavy metals), and mineral composition of the Barents Sea sediments, we aim to evaluate how the sedimentation environmental parameters are reflected in the elemental and mineral spatial and downcore distribution over the Late deglaciation and Holocene periods, including modern time.

The major goals of this study are:

- (1) to determine distribution of the grain-size fractions, mineral associations, multi-elemental (including the major, trace, and radiogenic elements) in sediment cores;
- (2) to determine the sedimentation rates in selected core of recent sediments;
- (3) to estimate distribution of heavy metals and their geochemical fractions in modern sediments;
- (4) to determine the grain-size and elemental composition in sediments deposited over the Late Deglaciation and Holocene periods; and,
- (5) to test selected elemental and mineral indicators for assessing the sedimentation environment in different areas of the Barents Sea.

## 2. Geologic Setting and Sedimentation Features

The Barents Sea is bordered by Svalbard and Franz Josef Land Archipelago on the north, the Novaya Zemlya Archipelago on the east, and the continental land (the Kola Peninsula and Pechora plain) on the south (Figure 1).

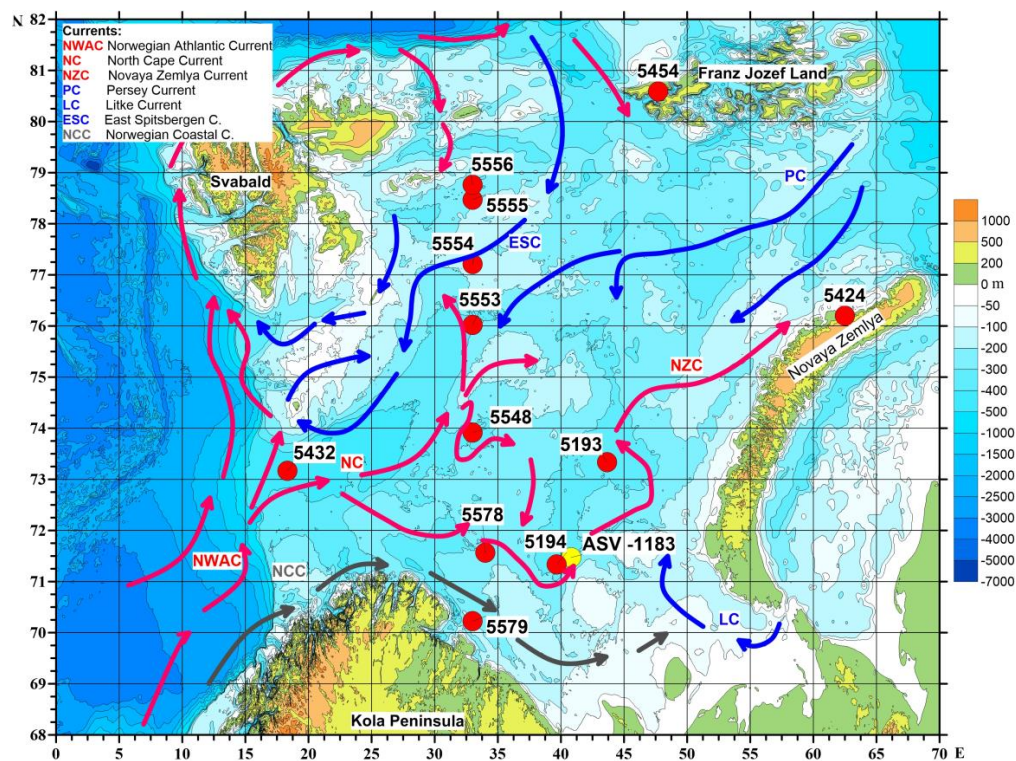


**Figure 1.** Scheme of location of sampled corer and directions of surface currents in the Barents Sea. Red and blue arrows mean relatively warm and cold currents, respectively.

The seafloor of the Barents Sea is generally flat, with a depth of less than 500 m. Only a few features are visible: relics of the latest phase of the ice age, during which large glaciers and meltwater carved their path in the sediments, but also deposited new sediments on top. The geology of the Barents Sea area can be explained by a complex combination of large-scale processes controlled by plate movements and varying climatic and depositional conditions during hundreds of millions of years of continental drift. The watershed of the Barents Sea has a different composition that is reflected in mineral source areas. Rocks of the Kola Peninsula are composed mainly of the Archean granite-gneisses, gabbro, and other basic rocks. In the Svalbard Archipelago, granitoids, volcanites of medium, and acid composition and traps are developed. In the Franz Josef Land, there are Jurassic and Cretaceous trappes, while, in the Novaya Zemlya Archipelago, Paleozoic sedimentary, igneous, and metamorphic complexes predominate: Triassic and Jurassic terrigenous deposits, as well as basalts and dolerites [4,30].

The Barents Sea is a glacier-affected epicontinental shallow basin. During the last glaciation, its shelf and surrounding archipelagoes were covered with the grounded Late Weichselian ice sheet [31–34]. During the Last Glacial Maximum (26.5 to 19 cal ka BP) the maximum of ice sheet extent occurred at 21 cal ka BP, when its northwestern area was covered with ice. Since that time, the dramatic paleoenvironmental changes happened induced by collapse of the continental ice sheets of the Northern hemisphere (deglaciation) that led to variations in the Atlantic water inflow, terrigenous material supply, biological productivity, and bottom current activity. Deglaciation was interrupted by relatively short periods of cooling and increasing the ice volume [35]. Late deglaciation was characterized by the processes of near-bottom transport and resuspension with the formation of laminated deposits by nepheloid flows, as well as of turbidites that are composed of largely fine-grained terrigenous material formed by the meltwater of retreating glaciers. The main deglaciation phase was accompanied by pulsed sedimentation from various gravity flows that result in the accumulation of distal glaciomarine facies comprising laminated clay and sand sequences with minor ice-rafted debris [4,14,36,37]. During the Holocene, normal marine sedimentation was mostly developed, several stages have been identified based on lithological and micropaleontological (foraminifera) data, reflecting changes in the intensity of Atlantic waters entering the Barents Sea [3,4]. According to radiocarbon dating by [38,39], the age of the Unit I (Holocene) bottom is 10–9.5 ka BP.

The seafloor of the Barents Sea is characterized by a combination of the elongated plateaus and depressions that are separated by narrow relatively deep troughs; through the latter, the relatively warm Atlantic water enters the Arctic Ocean. In the Barents Sea, as in other regions of the Western Arctic shelf, the terrigenous bottom sediments dominate (>80% of the area), where the main types are the terrigenous pelitic silts, which occupy more than 50% of its area. Sands and siltstone pelites amount in a total of less 32% of the bottom [14].

Sedimentary material enters the Barents Sea from various sources: glaciation centers such as the Svalbard, Franz Josef Land and Novaya Zemlya archipelagos, as well as the Transpolar Drift from the Laptev Sea and Central Arctic [17,40–42]. At the same time, increased concentrations of suspended particles and associated pollutants were observed along the edge of the melting ice [43]. An essential terrigenous source of sedimentary material is also related to the seafloor erosion, coastal abrasion, the cross-boundary atmospheric transport, and solid river runoff [30,44,45]. An additional supply of fine-dispersed suspended material through the Gorlo Strait from the White Sea is also of importance [41].

The modern hydrological situation in the Barents Sea resulted from the interaction of low-salinity Arctic water with warmer high-salinity Atlantic water (Figure 1). It carries pack ice from the Transpolar Drift during winter. Atlantic water from the North Atlantic by the warm surface Norwegian Atlantic Current, Norwegian-Northern Atlantic Current, which splits North of Norway into two branches. One, in the form of the North Cape Current and the other Norwegian Coastal current, enters the southern part of the Barents Sea through the Bear Island Trough, and further penetrates to the western coast of the Novaya Zemlya as a subsurface current. The boundary between transformed Atlantic water and



Arctic water represents the Polar Front that migrates between 74° N and 76° N and constitutes a major sinking and mixing area [46,47]. Sea-ice conditions are by strong seasonal and multiannual variability in position of the ice margin [48]. During the coldest years, the area east of 40° E is ice-covered up to the northeastern Kola Peninsula coast in winter, whereas the winter ice margin occurs at approximately 76° N during the warmest years.

Biogenous source of sedimentary material in the Barents Sea refers to an autochthonous suspended particulate material; the maximal total organic carbon (TOC) fluxes (up to 1200 mg C m<sup>-2</sup>·day<sup>-1</sup>) were recorded in the central part of the sea [49], wherein the warm and enriched in nutrients Atlantic water inflow. The total primary production of phytoplankton calculated from satellite observations and direct chlorophyll measurement, amounts 5.5 × 10<sup>7</sup> t·year<sup>-1</sup> of TOC, which is much higher when comparing to other Arctic seas [50]. Due to that, the Barents Sea, which amounts to only about 7% of the total area of the Arctic seas, contains the bulk of the Arctic marine biological resources [14]. In the Barents Sea, the present-day Polar Front (around 74–76° N) promotes the elevation of the primary production that resulted to rather high contents of TOC in modern sediments (to 2.5%, 1.9% on average); however, sediments are depleted in CaCO<sub>3</sub> (to 5.0%, 1.93% on average) [5,16,50]. The activity of phyto- and zooplanktic organisms is known to be an important source of sedimentary matter, as well as the suspended particulate matter (SPM) of various origin; besides, fine-dispersed SPM is supplied, as well as from the White and Kara Seas [41,51].

### 3. Materials and Methods

#### 3.1. Sediment Core's Location and Processing

The 11 sediment cores were raised by gravity corer (GC), multi corer (MUC), Neymisto tube (NT), and grab (GR) from the Barents Sea during the Shirshov Institute of Oceanology RAS Cruises 62, 67 and 68 of R/V Akademik Mstislav Keldysh in 2015, 2016, and 2017 years [52,53] (Figure 1).

The cores were recovered from the water depth ranged 122 to 638 m at the Central Deep (AMK-5193, -5194), Russkaya Gavan' Bay, at the northwestern coast of Novaya Zemlya (AMK-5424), the Bear Island Trough (AMK-5432), the Cambridge Strait, the Franz Josef Land (FJL; AMK-5454), and at the Kola oceanographic transect along the 33° E (AMK-5579, -5578, -5548, -5553, -5554, -5555, -5556; Table 1).

**Table 1.** The Barents Sea sediment cores studied in this work.

Core	Sampler	Latitude (° N)	Longitude (° E)	Cruise	Water Depth, m	Length, cm
5193	Niemisto	73.333	43.667	62AMK	328	37
5194	Gravity core	71.333	39.667	62AMK	353	450
5424	MUC	76.204	62.487	67AMK	176	24
5432	MUC	73.166	18.333	67AMK	462	25
5454	MUC	80.593	47.702	67AMK	638	33
Kola Transect (along ~33° N)						
5556	MUC	78.763	33.004	68AMK	360	32
5555	MUC	78.472	33.009	68AMK	122	29
5554	Grab	77.213	33.011	68AMK	160	5
5553	Grab	76.021	33.008	68AMK	297	14
5548	MUC	73.916	33.007	68AMK	322	28
5578	Grab	71.568	34.000	68AMK	235	17
5579	MUC	70.224	33.006	68AMK	248	30

Notation: MUC means multicorer.

Sediment core AMK-5194 (water depth 353 m, length 450 cm) was raised by GC from the southern part of vast Central Deep with depths of 200–350 m, which reflects the relief of the late Paleozoic Barents Sea's rift. The core was visually described and continuously sampled in 1-cm-thick sediment slices with intervals of 10 cm aboard the ship for lithological and geochemical studies.

The short cores of undisturbed sediments (maximum length 44 cm) were taken by MUC and NT, except AMK-5553, AMK-5554, and AMK-5578, which were sampled by GR. All of the short sediment cores were described and split into 0.5–1 cm (MUC and NT) and 5–10 cm intervals (GR) aboard the ship.

Core AMK-5193 (water depth 328 m, length 19 cm) was raised by NT nearby the AMK-5194 at the Central Depression. In the core AMK-5193, the occurrence forms (geochemical fractions) of some elements were studied. The MUC core AMK-5424 (water depth 176 m, length 24 cm) was collected from the deep part of the glaciated Russkaya Gavan' Bay at the northwestern coast of Novaya Zemlya. There, fine-grained suspended particles supplied by the Shokalsky Glacier meltwater ("glacier milk") [41], contribute to the mostly clay and silty-clay sediments of distinctively hydrodynamic calm environments. A large role in sedimentation is played by material that is brought from the inner-shelf areas, as well as transferred from shallow areas of the South-Western part of the Barents Sea. Core AMK-5432 (water depth 462 m, length 25 cm) was raised by MUC from the Bear Island Trough, with an unstable bottom current conditions that impact the sedimentation environment. A significant role in the supply of heterogeneous sedimentary material belongs to suspended matter brought with the North-Atlantic, North Cape and the East Spitsbergen Currents. Core MUC AMK-5454 (water depth 638 m, length 33 cm) collected from the deepest part of the Cambridge Strait was deposited under the influence of the Franz Josef Land glaciers and the coastal abrasion. Sediments of the Cambridge Strait are characterized by a predominance of fine-grained fractions that is a typical for the hydrodynamic calm deep-water environments.

The Kola Oceanographic Transect has about 700 km length and involves seven short cores (5–32 cm length) located along 33° E, with the water depths ranging from 122 m at South to 360 m at North (Figure 1, Table 1). This transect crosses the North Polar Front, which migrates around 70–72° N.

### 3.2. Methods

#### 3.2.1. Lithology

For GC AMK-5194 and MUC AMK-5424, -5432, and -5454 the sediment grain-size distribution was analyzed at intervals of 3–10 cm, respectively, by applying a combined sieving (>0.05 mm fractions), decantation (0.05–0.01 mm fraction), and pipette (0.01–0.005 mm, 0.005–0.001 mm, and <0.001 mm fractions) method developed by [54]. We used Bezrukov–Lisitzyn sediments grain size classification [55]: gravel/pebble (10–1 mm), sand (1–0.1 mm), silt (0.1–0.001 mm), and pelite (<0.01 mm). The AMK-5194 core physical properties were determined every 10-cm in 1 cm thick slices. To calculate water content (wetness) and bulk density, 10 cm<sup>3</sup> of preweighted wet sediment was freeze-dried while using the Alpha 2–4 LD plus freeze dryer, and then each sample was weighed again. Sediment colors were described according to the Munsell color chart system.

#### 3.2.2. Geochemistry

##### Elemental Analysis

The contents of major and trace elements (Al, Si, Ca, K, Fe, Mn, Ti, P, Cr, Sr, Zr, V, Ba) in 131 samples of bulk bottom sediments were determined by X-ray fluorescence (XRF) analyses of powdered and press-pelleted samples. Spectroskan (MAKS-GVM, SPEKTRON, St. Petersburg, Russia) equipped with vacuum spectrometry chamber (4 crystals LiF200, C002, PET, KAP, in the mode of 40 kV, from 0.50 to 2.0 mA) was used. Before the measurements, sediment samples were dried (at 105 °C over eight hours) and powdered in the Fritsch Planetary Mill Pulverisette 5/4 classic (Germany). The accuracy of measurements was controlled while using the certified reference material (CRM) SDO-1 (terrigenous oceanic clay), SDO-3 (carbonate sediment) and NIST-2703 (marine sediment). The accuracy varied within the limits of ±12%, reproducibility of major element analysis changed from 0.1% to 2.3%, while that for trace elements from 5.6% to 10.5%.

## Chemical Speciation

The analysis of physical-chemical speciation of Al, Fe, Mn, Cu, Cr, Co, Ni, and Cd in 42 samples was performed. It included the sequential extraction of the initial dry powdered samples (500 mg each) with reagents that allowed for separating elements with a different geochemical lability [56]. The leaching procedures were carried out in water-based ultrasonic disintegration treatment, at a sound frequency of 20 kHz. The following geochemical fractions (F) were leached from the bottom sediment samples: F-1—An exchangeable complex that consists of elements adsorbed mainly onto clays and associated with carbonates (the desorbing solution was acetate buffer (25% CH<sub>3</sub>COOH + 1 M CH<sub>3</sub>COONa) [57]; F-2—Authigenic Fe-Mn oxyhydroxides and related trace elements (the reduction reagent was 2 M NH<sub>2</sub>OH·HCl + 25% CH<sub>3</sub>COOH) [58]; F-3—Metals bound with organic matter and/or sulfides (the oxidation reagent was 30% H<sub>2</sub>O<sub>2</sub> + 0.1 M HNO<sub>3</sub> [59]; and, F-4—Residual or lithogenic (full acid decomposition with the mixture of concentrated HCl + HNO<sub>3</sub> + HF at 100 °C).

The first three fractions allow for estimating the contribution of geochemically labile metals, while the fourth one is a geochemically inert lithogenic form containing metals in crystal lattices of clastic and clay minerals. The effectiveness of the applied sequential extraction procedure was repeatedly tested by the European Community Bureau of Reference (BCR) [60–62]. Quantifying of the element concentrations in the sequential leached samples was carried out by method of Inductively Coupled Plasma-Mass Spectrometry (ICP-MS) Agilent 7500a [Agilent Technologies, Inc., Santa Clara, CA, USA]. The relative accuracy of trace elements measurements was controlled by the certified reference materials GSD-2 and GSD-6, estuarine bottom sediments, as well as SDO-1, terrigenous clay sediments. The difference between certificated and measured values ranged from 1% for major elements to 20% for trace elements.

### 3.2.3. Radionuclides

In 82 sediment samples from three MUC cores (AMK-5424, -5432, -5454), <sup>210</sup>Pb, <sup>226</sup>Ra, <sup>137</sup>Cs, and <sup>241</sup>Am were determined by gamma ray spectroscopy while using following gamma lines: 46.5 keV (<sup>210</sup>Pb), 609 keV (<sup>214</sup>Bi), 661.6 keV (<sup>137</sup>Cs), and 59.5 keV (<sup>241</sup>Am). Coaxial type HPGe detector GEM30P4-76 (Ortec) of relative efficiency 33% and energy resolution 1.69 keV (for 1332 keV line) was used for <sup>137</sup>Cs and <sup>226</sup>Ra determination in sediment samples AMK-5454 and -5432. Typical counting time was about 100,000 s. Planar HPGe detector GLP-36360/13P4 (Ortec) with a diameter of 36 mm and width of 13 mm was used for <sup>210</sup>Pb and <sup>241</sup>Am determination in sediment cores AMK-5424 and 5432. Typical counting time was about 300,000 s. HPGe detector GEM-C5060P4-B (Ortec) was used for the determination of all radionuclides in sediment core AMK-5424. Typical counting time was about 100,000 s. Sample masses vary from 10 to 40 g. Efficiency calibration was examined using standard reference materials IAEA-448, IAEA-447, and IAEA-315. The chronology of the cores was constructed by use of <sup>210</sup>Pb-based model.

### 3.2.4. Mineralogy

Mineralogical analysis of sedimentary material was carried according to the standard methods of XRD diffractometry [63,64] by use of D8 ADVANCE diffractometer (Bruker AXS), Cu-Kα, with Ni 0.02-filter, 40 kV, 40 mA, with linear detector LYNXEYE. Scanning in discrete mode in steps of 0.02° θ, exposure of 4 s/step in the range 2.0–70° 2θ, with rotation. For primary processing, interpretation of spectra, and calculation, the programs DIFFRAC.EVA, DIFFRAC.TOPAS (Quantitative Rietveld analysis, DIFFRAC.EVA V 5, DIFFRAC. TOPAS 5) was applied. Mass quantitative analysis was performed using corundum numbers from the ICDD database. The methods described were applied to identify clay minerals and determine their quantitative proportions.

The identification of clay minerals was performed on oriented air-dried samples prepared from the clay fraction suspension separated from the sample in distilled water [63,64]. Subsequently, samples were saturated with ethylene glycol (for the diagnosis of minerals of the smectite group, as well as

mixed-layered formations with swollen layers) and warmed at 550 °C (in cases of problems with the diagnosis of kaolinite and chlorite). Special cuvettes, being a kind of optical shutters for background scattering made of a single silicon crystal, were used for precision studies.

Full XRD analysis of the bulk sample was performed for the near-bottom suspension and sediment cores AMK-5424, -5432, -5454, where samples were taken over the entire core length, according to selected lithological horizons. In addition, sediments were analyzed in the central part of the Barents Sea (AMK-5417, 76°23'63" N, 51°00'00" E; 300 m depth; MUC; core length of 27 cm) and westward the Franz Joseph Land Archipelago (AMK 5452, 80°30'00" N, 43°38'02" E; 384 m depth, core length of 28 cm).

### 3.3. Data Processing

All of the calculations and statistical data processing were performed by use of the Statistica Trial software. They are, as follows: the graphs, map, lithological profiles, average values, Pearson correlation analysis (valid cases were presented for  $p = 0.95$ ), and coefficients of variation (CV).

## 4. Results

### 4.1. Lithology and Grain Size Distribution

Detailed grain size distribution was analyzed at the AMK-5194, -5424, -5432, and -5454 cores ( $n = 73$ ).

The AMK-5194 core was mainly composed of the clay (55.06–96.57%) and silty-clay sediments with an admixture of sand and gravel material (Figure 2). Down the core AMK-5194, total content of silt varied from 3.32% to 37.41%, sand and gravel fractions—0.10% to 21.20% and 0 to 0.09%, respectively. Median diameter (Md) varies from 0.8 to 5.6  $\mu\text{m}$  (Table S1). As a whole, sediments were moderately (So  $\sim 2$ ) or poorly (So  $> 3$ ) sorted, while deeper 290 cm, they were well sorted (So  $< 2$ ).

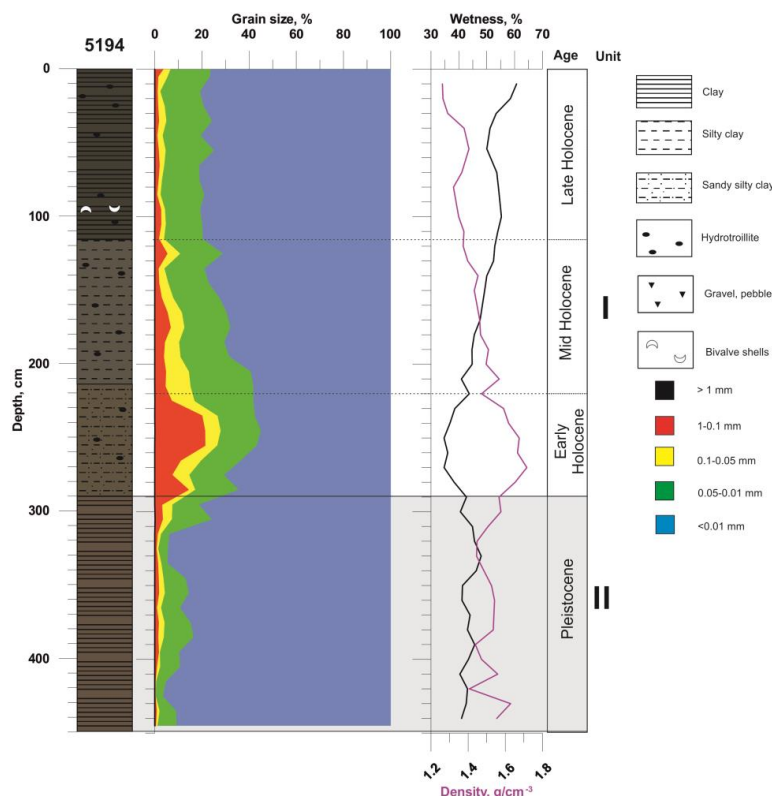


**Figure 2.** The lithology, grain size distribution, density, wetness, approximated age, and stratigraphic subdivision of the AMK-5194 sediment core, Central Deep of the Barents Sea.



The core AMC-5194 is located very close to the AMS  $^{14}\text{C}$  dated core ASV-1183 (71°28'30" N, 40°48'30" E, 330 m depth (Figure 1). In the ASV-1183 core, based on detailed lithological, microfossils and absolute age data, the two stages of paleoenvironmental development in the post-glacial period have been identified: Late Deglaciation (Stratigraphic Unit II) and Holocene (Stratigraphic Unit I) [2–4]. The core AMK-5194 was divided into the two Stratigraphic Units, II and I based on these data and our onboard lithological visual description, followed by the laboratory instrumental measurements (water content, density, grain-size analysis) (Figure 2).

Unit II Late Deglaciation sediments (290–446 cm) are composed of the finest clay sediments of dark gray-brown 2.5Y 4/2 to dark gray 10YR 4/1. The sediment density varied in this part of the column in the range 1.40–1.65 g/cm<sup>3</sup>, showing increased values in the deeper layers and correlating with the sandy-silt fraction. The sediments were characterized by a plasticity, uniformity, lack of bioturbation, rare diagenetic iron sulfide (hydrotroilite) inclusions, and feebly marked interlayers with a characteristic lamination, reinforced towards the core bottom. The clay-size material (<0.01 mm) was absolutely predominant (81.4–96.6%), wherein the finest clay (<0.001 mm) amounted from 61.1% to 72.8% of total sediment. The percentage of silt fraction varied 3.3% to 15.7%, while that of sand, from 0.1% to 3.06%. The Md ranged within the limits of 0.8 to 0.9  $\mu\text{m}$  and sediments are well sorted ( $\text{so} \leq 2$ ) (Table S1).

Unit I, Holocene sediments (0–290 cm) are presented by the thin olive-grey 5Y 4/2 silty-clay and dark grey 5Y 3/1 sandy-silt-clay material. The uppermost 10-cm layer was composed of oxidized sediment. Core sediments contain the rare hydrotroilite contractions, macrofaunal remains (bivalve shells, polychaeta tubes, single sponge spicules, and foraminifera). At the 165 cm depth, the olive-grey 5Y 4/2 silty-clay is changed to silty-clay with sand admixture, and at the 235 cm depth, to dark grey 5Y 4/1 sandy-silty-clay sediment. The clay fraction in Holocene sediments ranges from 55.06% to 81.23%, wherein the finest clay-size fraction (<0.001 mm) varied in limits of 29.9% to 57.4% (Table S1). The percentage of clay fraction changed a little to depth of 205 cm, while deeper it started to reduce and reached the minimum (55.6%) at the 255 cm depth. In the Holocene sediments, the silt fraction ranged from 16.78% to 37.41% with maximum at the 215–216 cm depth. In the upper part of the Unit I (0–215 cm), the sand fractions did not exceed 5.13%, while in the bottom part (165–290 cm) it increased and reached maximum of 21.2% at the 255 cm depth. In the interval of 225–245 cm, the single grains of gravel size were detected, while, at the lower boundary of Unit I (290 cm), the maximal density (1.7 g/cm<sup>3</sup>) was detected. Upward the core, density is gradually reduced to 1.2–1.3 g/cm<sup>3</sup>. Sorting of the Unit I sediments became worse due to an increase of the silt and sand percentage.

The Holocene Unit I is subdivided into three subunits, based on abundance of the organic remains and sand admixtures, which exhibited an opposite trend down the core 1. Late Holocene (0–115 cm): clay and silt sediments with abundant organic remains and the diagenetic iron sulfide (hydrotroilite) inclusions; 2. Mid Holocene (115–220 cm): silty-clay sediments with hydrotroilite patches; and, 3. Early Holocene (220–290 cm): sandy-silty sediments with the maximum sand content (21.2%) and the high density values (1.70–1.75 g/cm<sup>3</sup>) at 225–270 cm. Above the depth of 270 cm, the density decreases (to 1.23 g/cm<sup>3</sup>), while wetness increases reaching the maximum (61%) in the 0–10-cm layer (Figure 2).

Based on the closest location (Figure 1) and correlation of lithological characteristics of our AMK-5194 core and ASV-1183 core dated by AMS  $^{14}\text{C}$  [4], their synchronous sediment deposition in period of 10–13 ka BP, at the boundary of Early to Late Deglaciation, can be assumed. At that time, the sedimentation regime changed dramatically, due to multiple changes in the speeds of bottom nepheloid flows, which resulted in the appearance of thin-layered (laminated) textures with alternating of the brown (2.5 Y 4/2) oxidized and reduced grey (5Y 4/1, 5Y 3/1) interlayers, as well as turbidites. Brown layers reflect episodes of slowing or short-term interruptions of sedimentation [3].

Core AMK-5424, the Russkaya Gavan' Bay of the Novaya Zemlya Archipelago, was represented by generally uniform soft plastic mud of grey color (5Y/5/1), with hydrotroilite patches and remains of large tube worms. Grain-size analysis of this core has revealed a strong predominance of clay fraction (<0.01 mm), which amounted from 68% to 80% of total sediments, with a distinctly subordinate

proportion of silt (20–31%) and almost negligible to that of sand (0.05–1.44%) (Table S2). The uppermost layers were enriched in the thinnest material ( $<0.001$  mm) (Figure 3a).

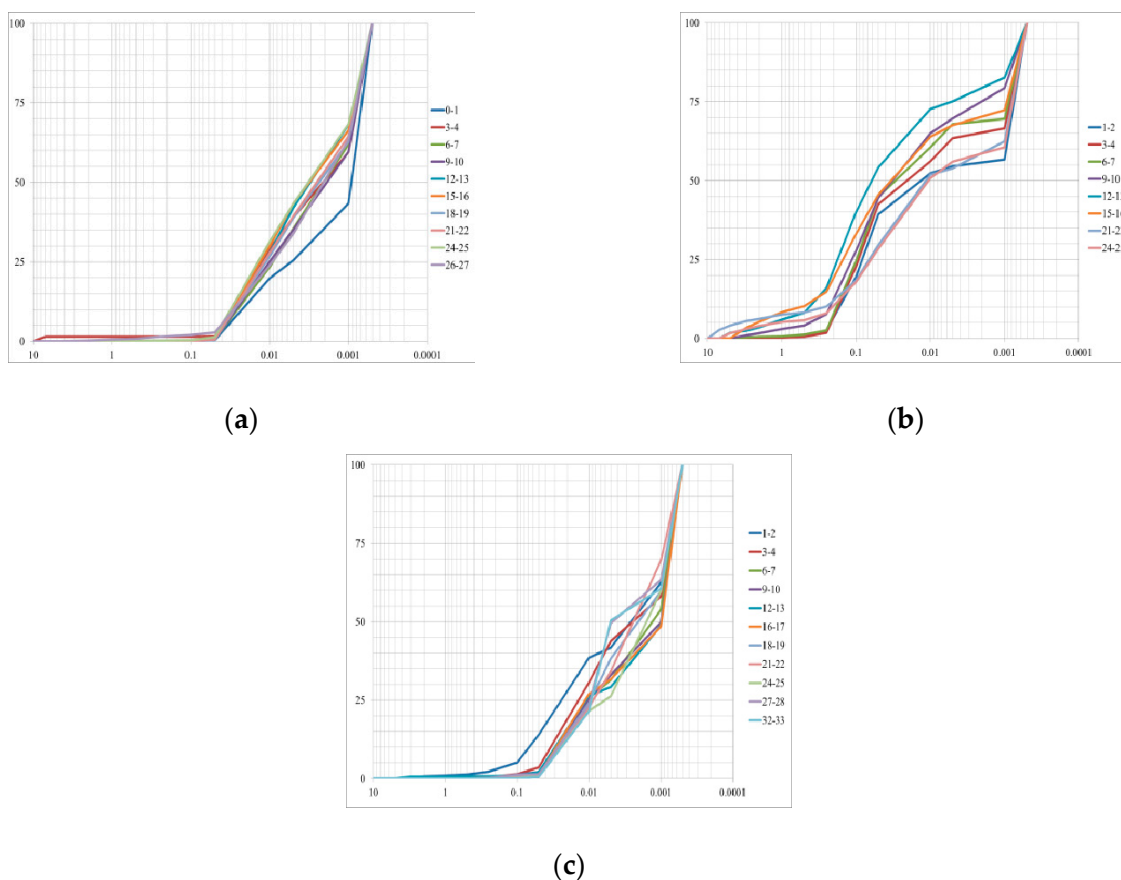


**Figure 3.** Percentage of grain size fractions (10–0.0001 mm) in sediment cores: (a) AMK-5424, the Russkaya Gavan' Bay, the northwestern coast of the Novaya Zemlya Archipelago; (b) AMK-5432, the Bear Island Trough; and, (c) AMK-5454, the Cambridge Strait, the Franz Josef Land. Different colors indicate sampling depths (cm).

Core AMK-5432 was raised from the Bear Island Trough, where modern sediments were deposited under conditions of the low to moderate unstable hydrodynamics. This sediment core is characterized by a mixed grain-size composition. Unlike AMK-5424 and -5454 cores, AMK-5432 core is enriched in sand (11–34%) and gravel (3–8.3%) fractions (Table S2). Down the core, the proportion of the coarse-grained material ( $>0.1$  mm) varied strongly, reaching the high and maximum values within the interval of 10–20 cm. Meanwhile, the proportions of clay (from 27% to 49%) and silt (25–36%) fractions show a rather weak change throughout the core (Figure 3b). The sorting coefficient  $So$  and median size  $Md$  varied widely due to the wide range of grain-size fractions.

Core AMK-5454, the Cambridge Strait, the Novaya Zemlya Archipelago, was composed of clayey–silty sediments, oxidized, dark gray-brown (10YR/4/2) or dark green-gray (Grey 1/3/10Y). Clay and silt fraction' content varied within the limits of 61.6% to 92.5% and 21% to 33%, respectively (Figure 3c). The  $Md$  values vary within the clay dimension (0.9–5.1  $\mu$ m). Values of  $So > 3$  suggest a poor sorting of sediments (Table S2). In the upper part of the core, there is a slight admixture of coarse-grained fractions: sand (up to 4%) and gravel (up to 1%) (Figure 3c). The rust patches, contractions, and bioturbation were found in sediments.

The Kola Transect. The investigated surface sediments (0–0.5 cm) are the silty clay, semi-liquid, with different portions of sand and even gravel, with rust spots, bioturbated, with color of 5Y 4/3 to 10YR 3/3 by the Muncell scale. They contain 39% to 86% of the clay-size fraction, whose proportion irregularly increased northward the transect. At places where the strong the North Cape and the Norwegian Coast Currents migrate, sediments are enriched in the coarse grained fractions from 5554 and 5578 stations: to 27% of gravel and to 43% of sand, respectively (Figure 4).

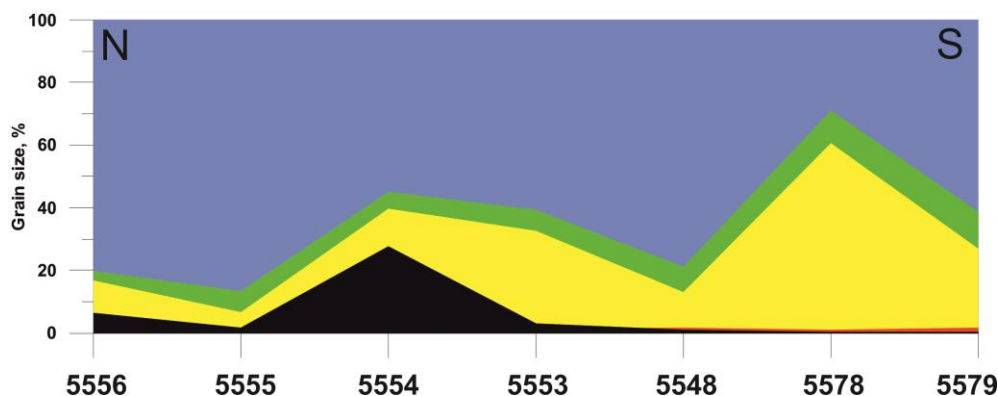


**Figure 4.** Grain-size composition in surface sediments from the Kola Transect along the 33°40' E, the Barents Sea. Symbols see in Figure 2.

#### 4.2. Radionuclides

Data of the gamma-spectrometry analysis are listed in Tables S3–S5. The mean sedimentation rates were determined by excess  $^{210}\text{Pb}$  using constant initial concentration (CIC) model [65,66]. This approach assumes a constant sedimentation rate and constant specific activity of deposited sediment. The mean sedimentation rate for 5454 was determined as 2.5 mm/year. The mean sedimentation rate for AMK-5432 core was determined by the  $^{210}\text{Pb}$  as 1.3 mm/year (Figure 5).

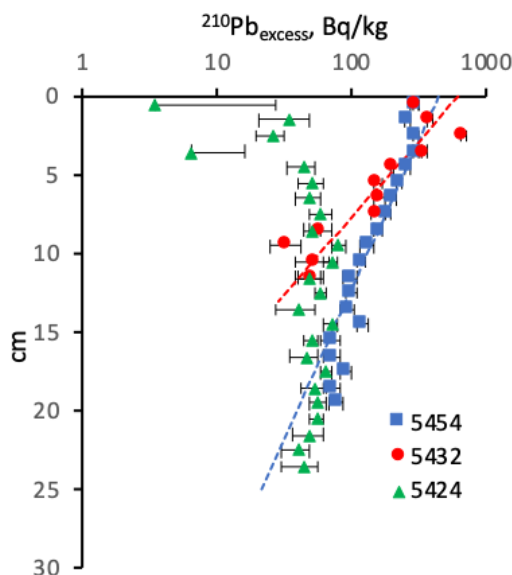


**Figure 5.** Excess  $^{210}\text{Pb}$  vertical profile from AMK-5424, -5432, and -5454 sediment cores.

To test the age model, we used two independent anthropogenic tracers— $^{137}\text{Cs}$  and  $^{241}\text{Am}$  (Figure 6). Unfortunately, the variability of sources and routes of  $^{137}\text{Cs}$  supply did not allow the age dating. The only stratigraphic marker is the beginning of the release of  $^{137}\text{Cs}$  (1952), but it is not reliable enough, since cesium can diffuse deeper into the sediment. Thus, we can obtain an upper estimate of sedimentation rate of 2.9 and 1.8 mm per year for AMK-5454 and -5432 cores, respectively.

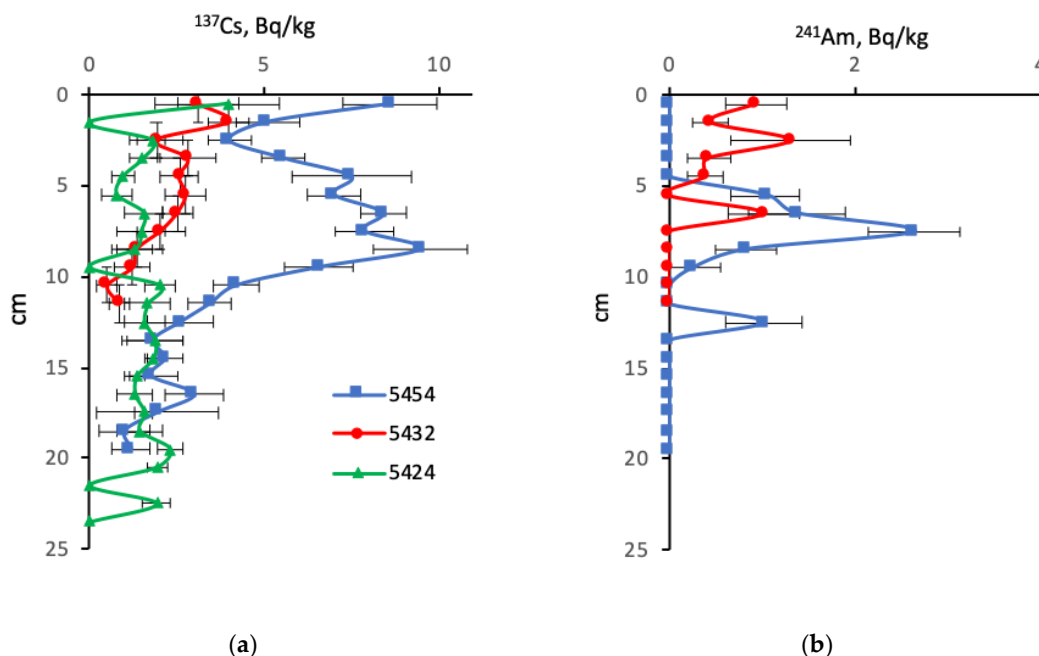


**Figure 6.** Downcore distribution of  $^{137}\text{Cs}$  (a) and  $^{241}\text{Am}$  (b) from AMK-5424, -5432, and -5454 cores.

#### 4.3. Mineralogy

The mineral complex diagnosed in the bottom sediments of the Russkaya Gavan' Bay (AMK-5424, Table 2) is almost invariable over the entire depth of the column in the range from 1 to 27 cm. The crystalline material of near-bottom suspension and bottom sediments is generally presented by one and the same mineral association, which includes muscovite, sericite, illite, and highly ordered Fe-chlorite, whose content reaches 48% (Table 2).

**Table 2.** Mineral composition of near-bottom suspension and bottom sediments of the AMK-5424 core according to XRD analysis.

Depth	Qz	K-Fsp	Ab	Ep	Cal	Dol	Ilt + Ms	Chl 2	Gp
(cm)	(%)	(%)	(%)	(%)	(%)	(%)	(%)	(%)	(%)
Suspension	25	3	11	n.d.	1	1	15	43	n.d.
0–1	22	3	12	1	1	1	11	48	n.d.
2–3	18	3	14	n.d.	n.d.	n.d.	26	32	6
19–20	22	3	13	n.d.	1	1	11	45	3
26–27	21	3	13	n.d.	1	2	12	46	1

Notation. Quartz—Qz, Albite—Ab, K-feldspar—K-fsp, Chlorite—Chl, Illite—Ilt, Muscovite—Ms, Calcite—Cal, Dolomite—Dol, Epidote—Ep, Gypsum—Gp, n.d.—not detected.

The diffraction profile has a full set of strong symmetrical reflections and a very low background, which characterizes well-crystallized substances with low defects and the absence of an amorphous component. The source of such material might be phyllites, clay, and crystalline shales, which are developed in the sedimentary rocks of the Northern Island of Novaya Zemlya Archipelago. This material



is transported to coastal areas by fresh and meltwater from the glaciers, followed by accumulation in the boundary zone as a result of avalanche sedimentation.

The mineral composition of sediment core from the Cambridge Strait (AMK-5454) is formed with the participation of basalts associated with trap magmatism of Franz Josef Land Archipelago (FJL). These rocks are highly unstable under influence of environmental factors and are easily decomposed. Pyroxenes, amphiboles, epidotes, and Ca-plagioclases supply the cations ( $\text{Ca}^{2+}$ ,  $\text{Mg}^{2+}$ , and  $\text{Fe}^{2+}$ ) for the authigenic mineral formation. Particles of the hydrodynamic active near-bottom layer may contain both the mineral complex derived from the FJL basalt complex, and not related to surrounding the FJL rocks. Thus, a wide range of minerals was diagnosed in the studied sediments: quartz (15–30%), acidic and basic plagioclases (8–42%), pyroxenes (2–11%), amphiboles, potassium feldspar, kaolinite (5–10%), chlorite (4–12%), illite (6–13%), and 12–13-Angstrom dioctahedral smectite containing monovalent interlayer cations  $\text{Na}^{1+}$ ,  $\text{K}^{1+}$ , 14–15-Angstrom smectite with bivalent interlayer cations  $\text{Ca}^{2+}$ ,  $\text{Mg}^{2+}$ , mixed-layered clays, Ca-zeolites (1–7%). It should be noted that the diffraction characteristics of registered zeolites (Mordenite, Ca-Heulandite, Clinoptilolite) correspond to the Ca-forms of these minerals. It means that the structural positions of freely bound cations are mainly filled with the  $\text{Ca}^{2+}$  cations supplied to the bottom waters as a result of basalt epigenesis. Here, the content of clay material is high, sometimes it amounts up to 47% in bulk sediment, the concentration of smectites in bulk sediments reaches 18% (Table 3).

**Table 3.** Mineral composition of near-bottom suspended matter (suspension) and sediments in the AMK-5454 core, of the Cambridge Strait, the Franz Josef Land Archipelago.

Depth	Qz	Ab	An	Ans	K-Fsp	Amp	Aug	Sme 12 Å	Sme 14 Å	Chl	Cln	Ilt	Gp	Zeo
(cm)	(%)	(%)	(%)	(%)	(%)	(%)	(%)	(%)	(%)	(%)	(%)	(%)	(%)	(%)
Suspension	27	12	8	n.d.	6	2	2	7	n.d.	12	10	13	n.d.	n.d.
0–1	20	n.d.	9	12	n.d.	n.d.	6	8	10	10	8	11	n.d.	5
1–2	26	n.d.	31	n.d.	n.d.	n.d.	9	n.d.	8	6	8	6	2	4
2–3	21	n.d.	35	n.d.	n.d.	n.d.	10	n.d.	10	5	5	6	1	6
3–4	22	n.d.	17	22	n.d.	n.d.	7	9	n.d.	6	6	8	2	1
4–5	25	n.d.	33	n.d.	n.d.	n.d.	6	10	n.d.	6	7	10	1	1
5–6	29	n.d.	35	n.d.	n.d.	n.d.	7	10	n.d.	4	5	8	1	1
6–7	27	n.d.	31	n.d.	n.d.	n.d.	7	9	n.d.	5	6	10	1	3
7–8	22	n.d.	30	n.d.	n.d.	n.d.	6	10	n.d.	7	7	11	1	6
8–9	21	n.d.	33	n.d.	n.d.	n.d.	10	10	n.d.	7	6	9	2	2
9–10	18	n.d.	42	n.d.	n.d.	n.d.	7	10	n.d.	5	6	9	2	1
10–11	21	n.d.	33	n.d.	n.d.	n.d.	9	11	n.d.	5	8	10	2	2
11–12	26	n.d.	22	n.d.	n.d.	n.d.	9	11	n.d.	6	8	13	2	3
12–13	22	n.d.	18	13	n.d.	n.d.	11	13	n.d.	6	7	9	n.d.	1
13–14	27	n.d.	25	n.d.	n.d.	n.d.	9	16	n.d.	6	7	10	n.d.	n.d.
14–15	15	n.d.	30	10	n.d.	n.d.	7	8	n.d.	6	7	11	1	5
15–16	16	n.d.	31	10	n.d.	n.d.	9	6	n.d.	5	5	10	n.d.	7
16–17	30	n.d.	16	14	n.d.	n.d.	9	9	n.d.	4	6	9	n.d.	2
17–18	24	n.d.	30	n.d.	n.d.	n.d.	6	14	n.d.	5	7	13	n.d.	1
18–19	22	n.d.	36	n.d.	n.d.	n.d.	5	9	n.d.	4	6	11	1	6
19–20	25	n.d.	26	n.d.	n.d.	n.d.	8	16	n.d.	7	8	6	2	2

Notation: Qz—quartz, Ab—albite, An—anorthite, Ans—andesine, K-fsp—K-feldspar, Amp—amphibole, Aug—augite, Sme 12 Å—smectite 12 Å, Sme 14 Å—smectite 14 Å, Chl—chlorite, Kln—kaolinite, Ilt—illite, Gp—gypsum, Zeo—zeolite, n.d.—not detected

An interesting feature of the mineral complex of near-bottom suspension from the Cambridge Strait, AMK-5454 core is the presence of albite, which was not registered in the deeper horizons, combined with 12-Angstrom smectite. Below the uppermost horizon, the 14-Angstrom smectites, and plagioclases of the basic composition were detected. These complexes, having the common origin, might be considered as paragenetic associations. Deeper the 3 cm, the smectite composition became averaged (Figure 7).

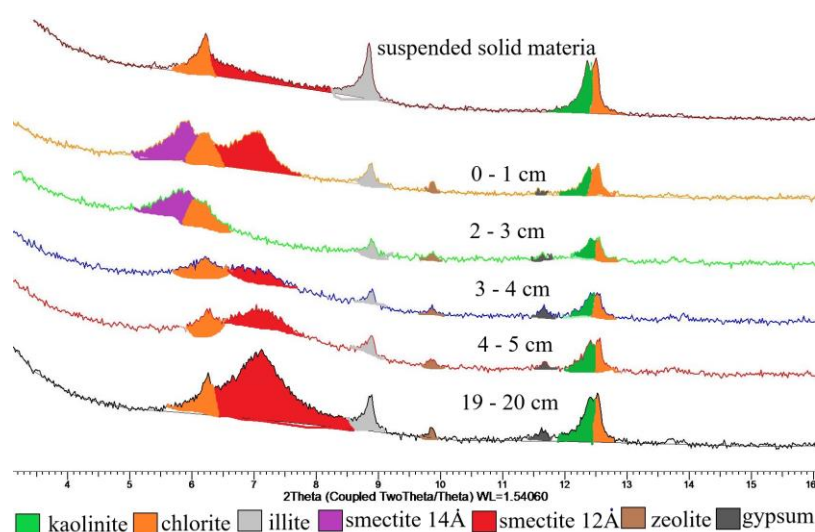


**Figure 7.** Variation of the clay mineral complex in the sediment core AMK-5454, the Cambridge Strait, the Franz Josef Land Archipelago.

The mineral composition of the clay fraction in sediment cores AMK-5454 (the Cambridge Strait, the Franz Josef Land Archipelago) showed a trend to decrease of the smectite content down the core (Table 4). In general, the clay mineral complex is composed of the four minerals (smectite, illite, kaolinite, and chlorite).

**Table 4.** Mineral composition of the clay fraction (XRD) in sediment cores of AMK-5432 (the Bear Island Trough), and AMK-5454 (the Cambridge Strait, the Franz Josef Land Archipelago).

Core	Depth (cm)	Smectite (%)	Illite (%)	Kaolinite (%)	Chlorite (%)
5432	1–4	8	54	19	19
5432	24	1	49	25	25
5454	1–4	39	32	15	14
5454	24	28	38	19	15

The mineral composition of bottom sediments taken for research to the west of the Franz Josef Land Archipelago (station 5452) is also marked by basalt deposits of nearby islands. With a distance to the west, in their complex, a total decrease in the content of clay minerals and their diversity is observed (Figure 3).

A characteristic feature of the sediment core AMK-5432, the Bear Island Trough, located at the Western boundary of the Barents Sea, is the occurrence of biogenic calcite, amounting to 7% (Table 5). Biogenic calcite was evidently caused by the deposition of the calcareous foraminiferal shells' detritus supplied by the North Atlantic Current.

**Table 5.** Mineral composition (XRD) of the near-bottom suspended particle (Suspension) and uppermost sediment layer (0–1 cm) of the core AMK-5432 (the Bear Island Trough).

Depth (cm)	Qz (%)	K-Fsp (%)	Ab (%)	Amp (%)	Aug (%)	Ms (%)	Ep (%)	Cal (%)	Dol (%)	Sme (%)	Ilt (%)	Chl (%)	Kln (%)	MLC (%)
Suspension	25	6	13	2	n.d.	8	3	7	1	7	10	11	7	n.d.
0–1	26	9	19	3	4	13	n.d.	4	1	n.d.	14	3	3	1

Notation: quartz—Qz, albite—Ab, K-feldspar—K-fsp, amphibole—Amp, augite—Aug, smectite—Sme, chlorite—Chl, kaolinite—Kln, illite—Ilt, muscovite—Ms, calcite—Cal, dolomite—Dol, epidote—Ep, mixed-layer clay—MLC, n.d.—not detected.

The mineral complex, diagnosed in bottom sediments core AMK-5432, is represented by quartz, feldspar, minerals of the amphibole and pyroxene groups, and micas. The group of clay minerals includes smectite, illite, kaolinite, and chlorite. The total content of clays is slightly lower than in other areas of the Barents Sea, and the sediments of some stations, smectite is completely lacking. Analysis of the clay fraction showed that, generally, the content of smectite and illite decreases with increasing depth, and kaolinite and chlorite increase (Table 4).

#### 4.4. Geochemistry

##### 4.4.1. Elemental Composition of the Surface Sediments

Elemental variations related to change in environmental conditions in different areas of the Barents Sea were studied based on geochemical data on the surface sediments sampled with MUC ( $n = 89$ ). Location of sampling sites and their parameters are displayed in Figure 1 and Table 1. There are, as follows: AMK-5424 (the Russkaya Gavan' Bay, the Novaya Zemlya Archipelago), AMK-5432 (the Bear Island Trough), AMK-5454 (the Cambridge Strait, the Franz Josef Land), as well as seven stations located at the Kola meridional transect along  $\sim 33.400^\circ$  E. All of the XRF data on the sediment cores studied are shown in Tables S6–S8.

In Table 6, contents of chemical elements in surface sediments (0–5 cm) of the Barents Sea, are listed in comparison to the Upper Continental Crust (UCC) values [67], as well as to the regional background heavy metal averages [21]. Based on the chemical composition, sediments under consideration can be ranked among the terrigenous sediments, whose typical Si/Al ratio is more than 3. By content of Si, Al, Fe, Mg, and Ti, they differ insignificantly from the UCC values. However, these sediments are significantly depleted in Ca, Sr, Cr, Ni, and enriched in Mn, V, and As.

**Table 6.** Minimal, maximal, and average element contents in the surface sediments of the Barents Sea.

Element	C min	C max	C aver	UCC [67]	Regional Background [21]
C org, %	0.49	1.76	0.98	-	-
Al, %	7.12	9.52	8.30	7.96	-
Si, %	24.21	29.58	27.28	28.8	-
Fe, %	3.92	9.35	4.43	4.32	-
Ca, %	0.60	1.45	0.84	3.85	-
Ti, %	0.34	0.50	0.43	0.40	-
Mg, %	1.53	1.99	1.79	2.20	-
Mn, %	0.03	0.89	0.27	0.07	-
V, mg/kg	89	202	140	98	-
Sr, mg/kg	141	168	157	333	-
Zr, mg/kg	132	209	165	203	-
Ba, mg/kg	188	479	439	584	-
As, mg/kg	2	28	19	8	-
Cr, mg/kg	70	128	85	126	70
Zn, mg/kg	37	97	69	65	150
Pb, mg/kg	15	31	18	15	30
Cu, mg/kg	24	47	31	25	35
Ni, mg/kg	29	51	39	56	30
Co, mg/kg	6	33	20	24	12

Total contents of heavy metals Zn, Cu, and Pb, which are potentially toxic for the bottom fauna, are mostly lower than background regional values for the Barents Sea sediments (Table 6). At the same time, in majority of our samples, the Cr concentration is 20% higher than the regional background value, and, in almost all samples, Ni and Co contents are 30–60% higher than the background values. The contents of potentially toxic metalloid As vary noticeably, from 2 to 28 mg/kg, with rather high average content (19 mg/kg). However, there are no published data on the regional As background values.

The analysis of paired correlations ( $R^2$ ,  $p < 0.05$ ) (Table S9) revealed a significant positive relationship as follows: lg Md-Si/Al (0.69), Si-Zr (0.85), Al-Mn (0.81), Al-Cr (0.95), Al-Cu (0.86), Al-Ba (0.57), Fe-Mn (0.81), Fe-Zn (0.71), Zn-Cu (0.71), Cu-Mn (0.88), and As-Mn (0.83). A significant negative correlation was found for Si-Al (−0.92), Al-Zr (−0.66), Zr-Mn (−0.75), Zr-Fe (−0.69), Si-Mn (−0.94), Si-V (−0.71), and Si-Cu (−0.97). Aluminum and majority of trace elements (except Zr) showed no correlation with Si. The Zr is commonly included in the accessory mineral zircon. Zircon has a high hardness value and it is characterized by an increased content in sand fraction, wherein the abrasion-resistant quartz and frame aluminosilicates are also dominated. The correlation coefficients between Mn and Fe in all samples are quite high ( $R^2$  0.81), which emphasizes the similarity of their geochemical behavior in surface sediments. In addition, these elements show significant positive correlations with Al, which is a structural element of layered clay minerals, in particular, montmorillonite, chlorite, and illite. It should be noticed that most heavy metals (Co, V, Pb, As, Cu, and Zn) correlate with Fe and Mn, the intermediate position is occupied by Cr and Ni which show a positive correlation with both Al, Ti and Zr, and Fe, Mn.

Along the Kola Transect, the sea depths vary between 122 and 360 m (Table 1), the deepest station AMK-5556 is located at 76°76′30″ N. At seven stations from the Kola Transect, the major and selected trace elements were analyzed by the XRF method in the surface sediments that were collected by MUC (Table S7). In Figure 8, the variations in element contents are displayed. A sharp increase in Si, Ba, and Zr contents (Figure 8a,b) corresponds to maximum of sand fraction (43%) at station AMK-5578. In sediments of AMK-5578, -5579, located in the shallow area, with increased contents of silt and sand fractions, the maximal Ca content was detected (Figure 8c). Along the profile, Ca content showed a regular growth from 0.73% in the northern part (AMK-5556), to 1.45% in the southern ones (AMK-5579). Manganese shows an opposite to Ca trend: decrease from northern to southern portion of transect, it may suggest a predominant Mn accumulation in the fine-grained clay fraction. The concentrations of Al, Fe, Sr, Rb, V, and Ti vary within  $\pm 20\%$  from their mean values, exhibiting a quite stable distribution within the sediment profile.

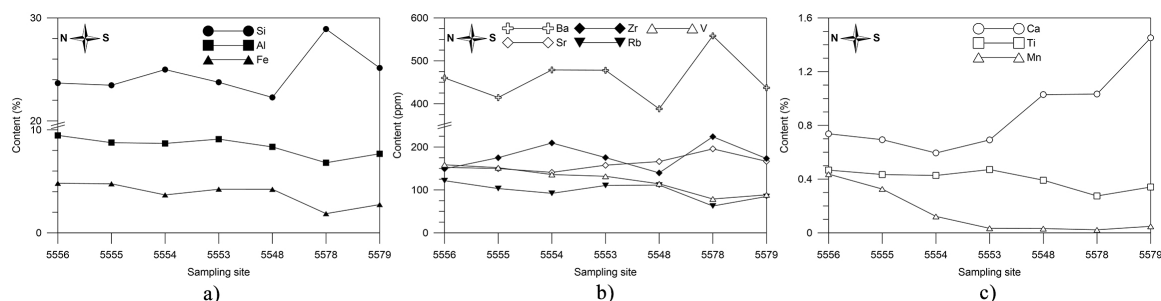


**Figure 8.** Variation of element concentrations in surface sediments at the Kola Transect along 32.400° E, the Barents Sea. Elements: (a) Si, Al, Fe; (b) Ba, Zr, Sr, Rb; (c) Ca, Ti, Mn.

#### 4.4.2. Major and Trace Elements' Distribution in Sediment Cores (Sampled with GC and MUC)

Table 7 lists the average elemental contents and selected ratios of elements in cores taken from the Central Deep (GC, AMK-5194), the Russkaya Gavan' Bay, the Novaya Zemlya Archipelago (MUC, AMK-5424), the Bear Island Trough (MUC, AMK-5432), and the Cambridge Strait, the Franz Josef Land Archipelago (MUC, AMK-5454).



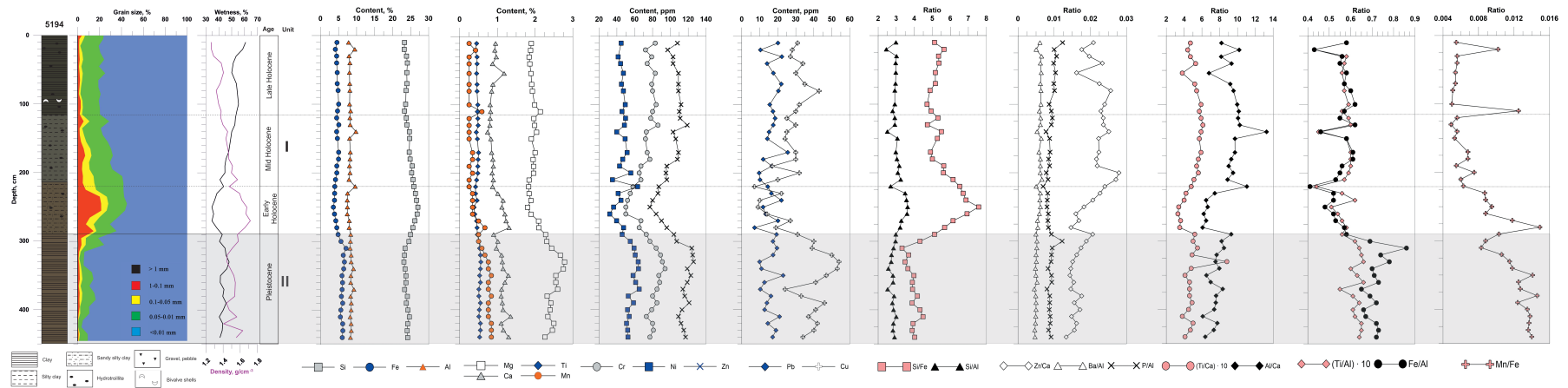
**Table 7.** Average contents and ratios of elements in sediment cores AMK-5194, -5424, -5432, and -5454 in comparison to the Upper Continental Crust (UCC) [67].

Element	Central Deep 5194 (n = 42)	Russkaya Gavan' Bay 5424 (n = 24)	Bear Island Trough 5432 (n = 25)	Cambridge Strait 5454 (n = 33)	UCC [67]
Si, %	24.41	25.61	30.37	21.12	28.8
Al, %	8.29	8.39	6.33	7.40	7.96
Fe, %	5.07	5.06	2.67	8.87	4.32
Ca, %	1.02	n.d.	n.d.	n.d.	3.85
Mg, %	2.15	n.d.	n.d.	n.d.	2.20
K, %	2.80	2.18	1.78	1.42	2.14
Ti, %	0.48	0.47	0.32	0.71	0.40
P, %	0.09	0.07	0.07	0.21	0.08
Mn, %	0.05	0.05	0.04	0.79	0.07
Zr, ppm	193	189	230	104	203
Sr, ppm	165	140	170	215	333
Ba, ppm	449	n.d.	n.d.	n.d.	584
Zn, ppm	107	91	47	108	65
Cr, ppm	75	53	44	51	126
Co, ppm	19	n.d.	10	n.d.	24
Ni, ppm	50	n.d.	33	n.d.	56
Cu, ppm	31	34	27	199	25
Pb, ppm	16	n.d.	13	n.d.	15
Si/Al	2.96	3.06	4.81	2.82	3.61
Si/Fe	4.81	5.06	11.37	2.38	6.67
Fe/Al	0.61	0.60	0.42	1.20	0.54
Ti/Al	0.06	0.06	0.05	0.10	0.06
Ti/K	0.17	0.22	0.18	0.51	0.19
Mn/Fe	0.009	0.009	0.013	0.090	0.016
P/Al	0.010	0.009	0.011	0.030	0.010

In the sediment core GC AMK-5194, taken from the Central Deep (Figure 1, Table 1), the elemental composition was determined by XRF analysis (data are listed in Table S8). The mean contents of Si, Al, Mg, Co, Ni, and Pb show less differences when comparing to the UCC mean value UCC (Table 7). These sediments are strongly (2–4-fold) depleted in Ca, Sr, and Cr. An extremely low Ca content (1.02% on average) corresponds to the low  $\text{CaCO}_3$  content (2.49% on average), which confirms a generally noncalcareous sediments of the Barents Sea as a whole, in the Central Deep particularly. Meanwhile, the mean contents of Al, K, and Zn are noticeably higher than that in the UCC.

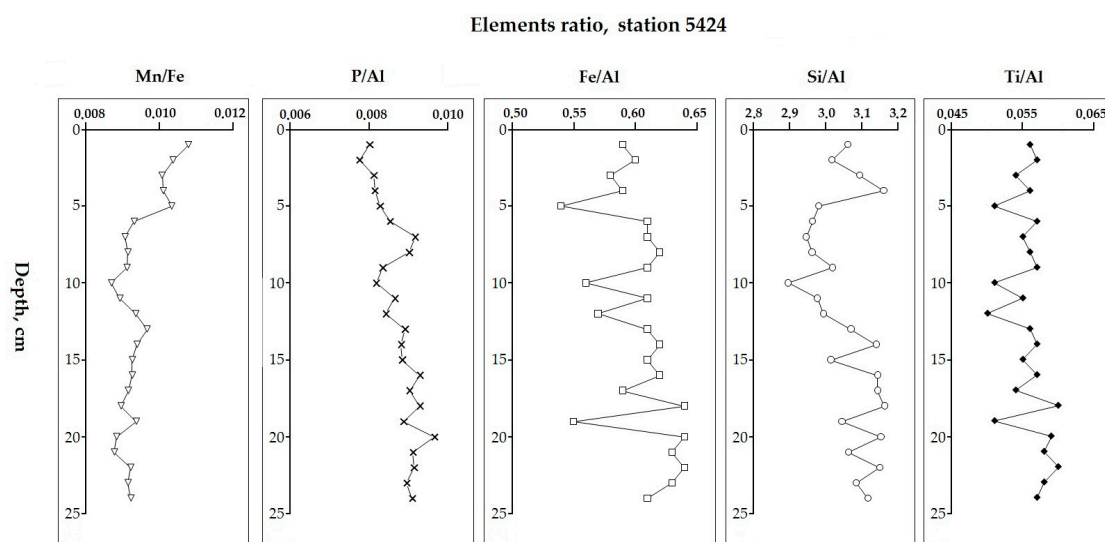
The downcore AMK-5194 variability of elemental composition was estimated by the use of coefficients of variation CV according to the formula:  $CV = \sigma/\bar{x} \cdot 100\%$ , where  $\sigma$  is a standard deviation,  $\bar{x}$  is a mean value. The major elements (Si, Al, K, Mg, Ti), along with Zr, Ba, Sr, Zn, and Cr, showed an insignificant variability ( $CV \leq 13\%$ ). A CV values between  $>13\%$  and  $<33\%$  indicates the moderate variability of Fe, Zn, Cr, Ca, and Pb. The CV values higher than 33% suggest that elements (Cu, 36% and Mn, 48%) are significantly variable. The high variability of Cu and Mn may be directly related to their elevated geochemical mobility.

Figure 9 displays the distribution of elements and elements ratios down the core AMK-5194. They showed no significant vertical differentiation of major elements Si, Al, Fe, Ti, Ca, Mg, whose variations are less prominent than that of the heavy metals Cr, Zn, Ni, Cu, and Pb. When comparing the downcore distribution of elements with that of grain-size composition (Figure 2), one may notice the increased Si contents correspondingly to the elevated values of sand ( $>0.1$  mm) fraction in the 240–290 cm thickness. In these layers, reduced contents of Mg, as well as Cr, Zn, Ni, Cu, and Pb, were recorded, and their minimal contents coincide with the sand fraction maximum (22%) at depth of 260 cm. In contrast, sediments deeper 290 cm with increased content of clay fraction are relatively enriched in Mg and heavy metals.



**Figure 9.** Lithology and variations of Si, Al, Fe, Ca, Mg, Ti, Mn, heavy metals Cr, Zn, Ni, Cu, and Pb, as well as elemental ratios in core AMK-5194, the Central Deep of the Barents Sea.

In the Russkaya Gavan' Bay, core AMK-5424, distribution of elements exhibits no sharp change (Table S6), which evidently reflected a strong predominance (68–80%) of the clay fraction with subordinate proportion of silt (20–31%) and admixture of sand and gravel (Figure 10, Table S2). Mean values of Si/Al, P/Al, Fe/Al, and Ti/Al ratios displayed a slight variation around their mean values for the core and no significant difference with that for UCC. The exception is the Mn/Fe ratio, which showed a noticeable growth in the uppermost 5-cm layer, and its mean value is about 30% lower than that of the UCC (Table 7).



**Figure 10.** The elemental ratios down the core AMK-5424, the Russkaya Gavan' Bay, Novaya Zemlya Archipelago. Dotted line means element ratio's average for the core.

Down the core, these ratios showed a slight variation around their core average values: Mn/Fe (0.009), P/Al (0.009), Si/Al (3.06), Ti/Al (0.06), and Fe/Al (0.60) (Figure 10). The Si/Al ratio peak in horizon of 3–4 cm is possibly caused by an admixture of sand and gravel (1.5%). Findings of authigenic Fe sulfide (hydrotroilite patches) and organic debris (large worms) in the soft mud of grey color (5Y/5/1), indicate the processes of early diagenesis. A noticeable growth of Mn/Fe in the upper 0–5 cm reflects an intensification of the oxygen dynamics in bottom water. The Mn/Fe and P/Al ratios' distributions display no coincidence, since the Mn/Fe grow occurs under oxygenated conditions, while an increase in the P/Al ratio mostly reflects the biogenic associated material, whose decomposition contributes to the oxygen consumption. The similar patterns of the Fe/Al and Ti/Al values may suggest their more silt-specific character in this core.

Core AMK-5432, the Bear Island Trough, is mostly composed of the sandy–silt fraction, totaling 52% to 65% of bulk sediment. A significant contribution (18–40%) of the coarse-grained (>0.1 mm) material (sand and gravel) (Table S2) is likely reflected in high contents of Si (30.37%) and Zr (230 ppm), as well as a rather high Si/Al mean ratio (4.81) (Table S6). Along with the reduced Al (6.33%) and Fe (2.67%) mean contents, these evidently suggest a terrigenous character of the core AMK-5432. The peak Si/Al (5.8) value was recorded in the 1–2 cm layer, wherein the clay fraction and Al content increased, and sand fraction decreased (Table S2). The high average values of Si/Al ratio could also be associated with biogenous material in sediment layers, enriched in bioSiO<sub>2</sub> (opal), as soon as many species of diatoms thrive in the Arctic environment. That confirms the earlier data on distribution of opal, whose content was >1% in modern sediments of the Western Arctic sediments [16]. The diagenetic oxidation occurs here based on sharp growth of Mn/Fe ratio in the upper layer, which possibly promoted the elements' redistribution process. The mean values of Mn/Fe, P/Al, Fe/Al, and Ti/Al ratios display a variation within the limits of 5% to 22% when comparing to those for UCC (Table 7).

Down the core AMK-5432, a rhythmic variation in Fe/Al, Si/Al, and Ti/Al ratio was detected (Figure 11). In the upper 0–5 cm layer, an opposite trend in change of Si/Al, on the one hand, and Mn/Fe and P/Al, on the other hand, is distinctly seen. A growth in the Mn/Fe in the 0–4-cm layer likely indicates the early diagenesis, while an increase in the P/Al ratio reflects an increased proportion of biogenic over clay components. Variations of these both ratios are evidently related to early diagenetic changes in sediments.

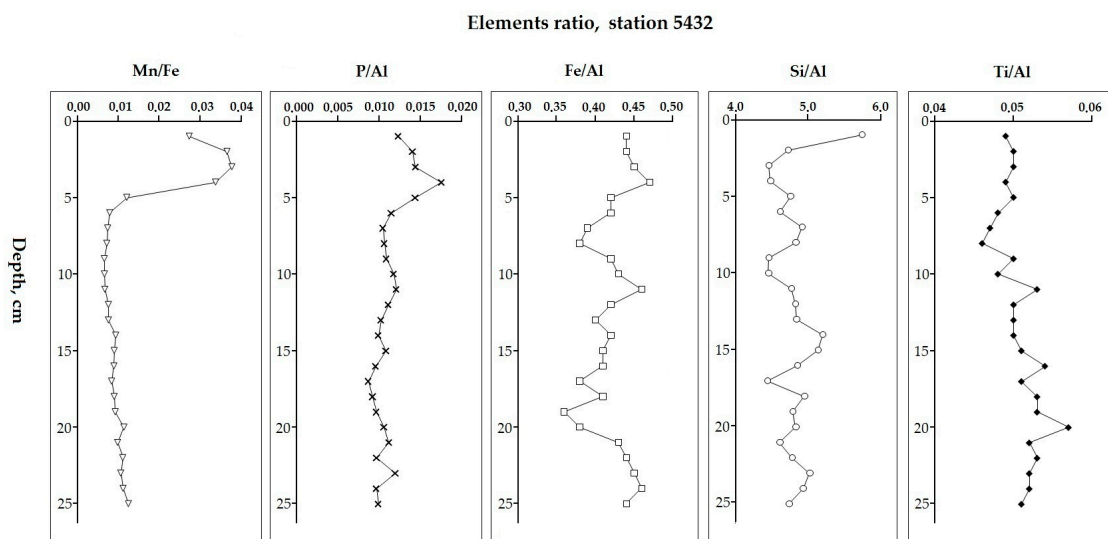


**Figure 11.** The elemental ratios down the core AMK-5432, the Bear Island Trough. Dotted line means element ratio's average for the core.

Sediments of core AMK-5454, the Cambridge Strait, the Franz Josef Land Archipelago, are enriched in Ti (0.71%), Fe (8.87%), P (0.21%), Zn (108 ppm), Cu (199 ppm), and particularly, in Mn (0.793%) comparing to UCC, as well as mean values of Mn/Fe, P/Al, and Fe/Al ratios are six, three, and two times more (Table 7). Unlike these, the mean content of Si (21.12%), as well as the Si/Al (2.82) ratio are noticeably lower relatively the UCC (Tables 6 and 7). The Fe/Al ratio in combination with Mn/Fe ratio suggests an average composition close to that of average deep-sea clays. From bottom to top of this core, the different trends of Mn and Fe distribution can be seen: The considerable Mn rise versus a rather weak Fe change (Table S6). That suggests a different mobility of Mn and Fe during the early diagenetic processes, which resulted in the sharp rise of Mn/Fe ratio in the 0–8 cm layer, while peaks of P/Al and Fe/Al ratios are recorded in the low part of the core (Figure 12).

#### 4.4.3. Trace Metal Speciation

Core AMK-5193 is composed of the Upper Holocene sediments, which are characterized by absolute predominance of clay fraction (90% on average). The uppermost (0–2 cm) oxidized layer of the brown color is provided by a rather high oxygen concentration (5.9 mol/L) in the bottom water. In the deeper sediment layers, hydrogen index (pH) values ranged from 7.0 to 7.9 (Figure 13).



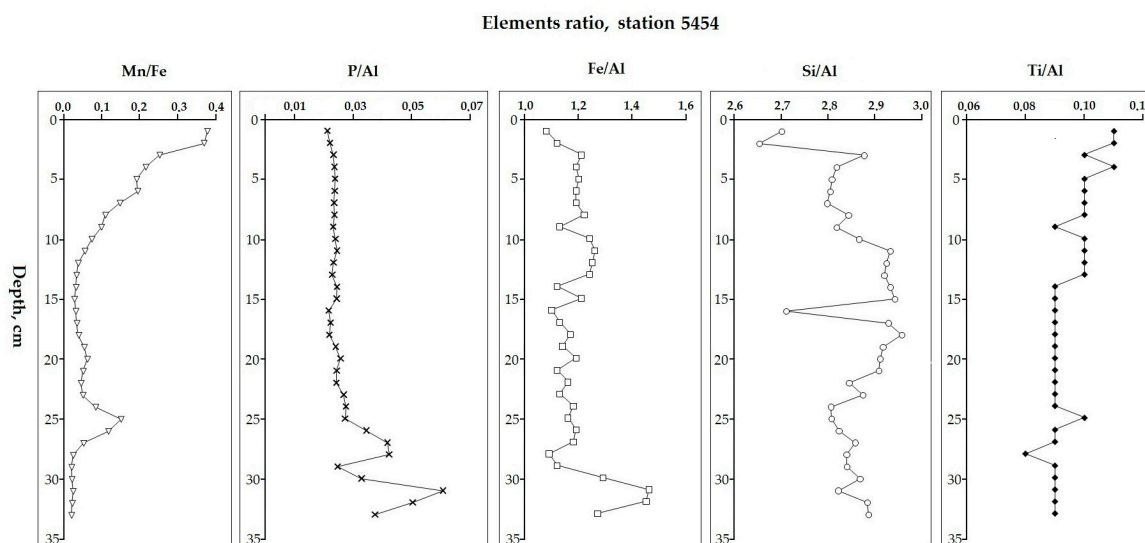


**Figure 12.** The elemental ratios down the core AMK-5454, the Cambridge Strait, the Franz Josef Land Archipelago. Dotted line means element ratio's average for the core.

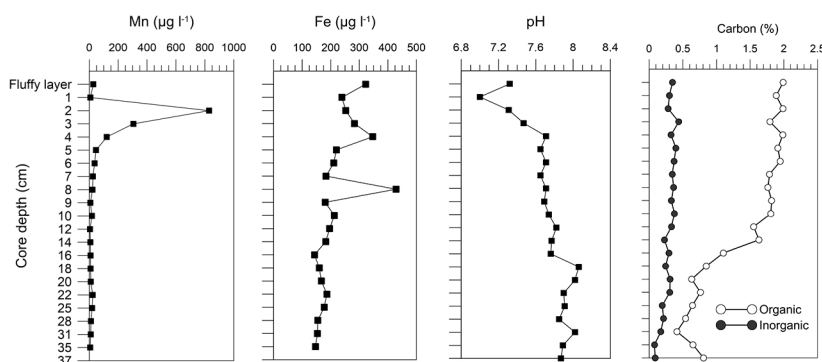


**Figure 13.** Concentrations of dissolved Mn (a), Fe (b), and pH values (c) in the pore water, as well as, the  $C_{org}$  and  $C_{carb}$  content in sediments (d) of core AMK-5193, the Central Deep of the Barents Sea.

Down the core, the environment became slightly alkaline, oxidized sediments were replaced by the gray-brown, and deeper—by the gray silty pelite with sandy admixture. Below horizon of 6 cm, hydrotroilite concretions ( $FeS \cdot nH_2O$ ) were found, which obviously indicated an early stage of diagenetic processes induced by organic matter oxidation under conditions of elevated  $C_{org}$  content (up to 2%) and rather high wetness (up to 77.34% in the Suspension). As a whole,  $C_{org}$  showed a trend to a two-fold decrease in the lower parts of the core, while a noticeable drop was detected at depth of 14 cm. (Figure 13).

The following geochemical fractions were leached from the bottom sediment samples: F-1—An exchangeable complex which consists of elements adsorbed mainly onto clays and associated with carbonates; F-2—Authigenic Fe-Mn oxyhydroxides and related trace elements; F-3—Metals bound with organic matter and/or sulfides; and, F-4—Residual or lithogenic (Table S10).

Our data on element speciation in core AMK-5193, for the first time, have revealed an absolute majority of the geochemically inert lithogenic fraction of Al (on average 97% total content) throughout the core length. Similar results were obtained for Fe, Cr, and Ni (70–90%) (Figure 14a,b,e). In the upper layers (to 5 cm), Fe is approximately equally shared between lithogenic form and the sum of mobile ones, while a proportion of Fe fraction, bound to organic matter, is increased to 20% of the total content. It should be noted that, according to the lithological description, in core AMK-5193, the authigenic iron sulfide (hydrotroilite) patches were found, which suggested the partial inclusion of Fe-3 form in hydrosulfides generated during sulfate reduction. Down the core, the growth of lithogenic fraction of

Fe-4 was detected, making up about 80% of its total content. The proportion of adsorbed fraction Fe-1 was of minor significance.

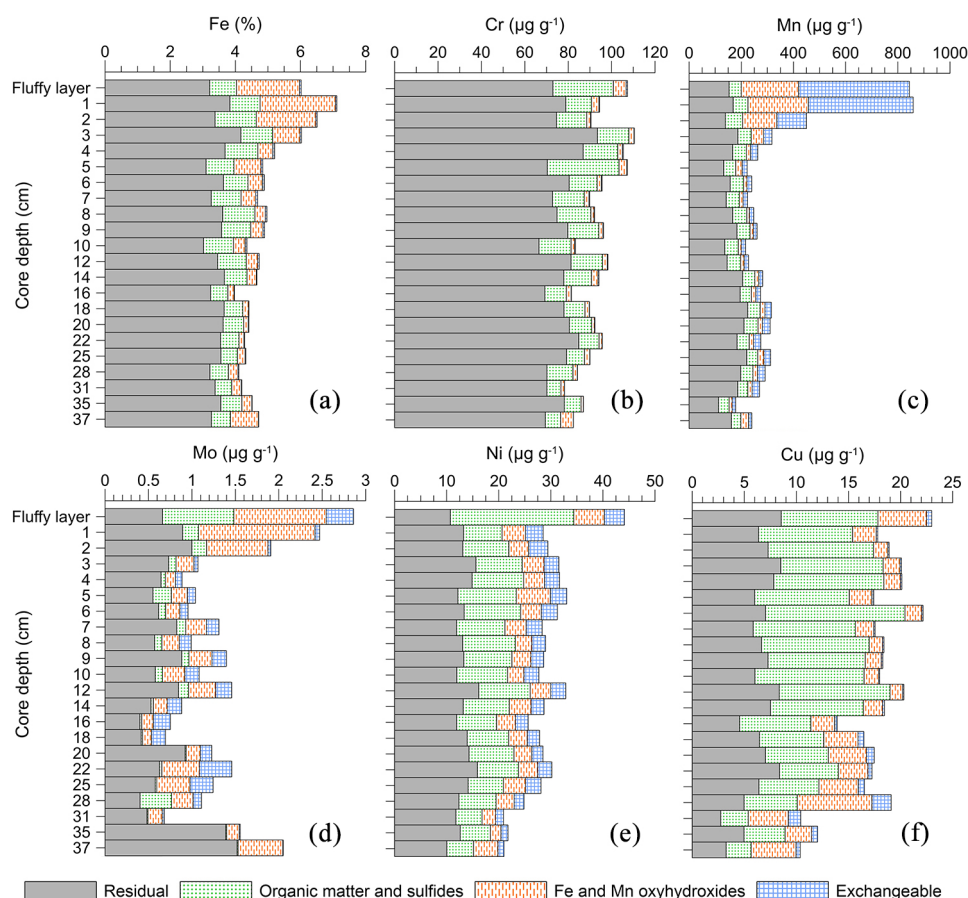


**Figure 14.** Downcore variation in the geochemical fractions of Fe (a), Cr (b), Mn (c), Mo (d), Ni (e), and Cu (f) in the AMK-5193 core, Central Deep of the Barents Sea.

The total Mn content in the upper oxidized layer (850 µg/g) is close to the Clarke value in sedimentary rocks. At the sediment horizon of 4 cm, the Mn total content decreased sharply when compared to the Suspension. An opposite behavior was revealed for dissolved Mn in pore water: at the horizon of 1–2 cm, it sharply increased by more than 100 times, up to 830 µg/L (Figure 13). In the surface layer (0–2 cm), an absolute predominance of geochemically mobile Mn forms was found (80% of the total content), wherein the authigenic Mn oxy-hydroxides and exchangeable (adsorbed/bound to carbonate) Mn forms amounted about 30% and 50%, respectively (Figure 14c). In sediments deeper 4 cm, the lithogenic Mn form (Mn-4) prevailed: to 70% of total content. Mo, which is associated with the Mn oxy-hydroxides (Mo-2 form) in the surface layers, decreases sharply: from 1.06 to 0.21 µg/g (i.e., by five times) (Figure 14c). That was obviously due to Mo desorption from the Mn oxy-hydroxides during the Mn (IV) reduction; down the core, Mo and Mn revealed the synchronous distribution. The Mo and Cu (Figure 14d,f) are characterized by the greatest proportions of fraction, bound to organic matter, the Mo-3 and Cu-3 forms count 35–50% of total content on average, where the  $C_{org}$  content >1.5%. Moreover, these metals show the closest relationship with  $C_{org}$  throughout the core: Cu- $C_{org}$ ,  $R^2 = 0.90$  and  $0.74$ , respectively;  $p = 0.05$ ).

It should be noticed the significant essential contribution of geochemically mobile fractions (sum of exchangeable, associated with authigenic Fe-Mn oxyhydroxides and organic matter) to accumulation of Ni, Pb, Co, Mn, Mo, and Cu, whose proportions within the upper sediment layer of 0–10 cm reached up 70% of total content of each metal. The downcore distribution of Cd and Pb is characterized by an

increased (comparing to Cu) proportion adsorbed form on both clay minerals (F-1) and authigenic Fe-Mn hydroxides (F-2); with significant positive correlation ( $R^2 = 0.85$ ;  $p = 0.05$ ).

The contribution of the lithogenic fraction to accumulation of Co, Cu, Cd, and Pb in sediment core AMK-5193 varies from 65% (Co) to 30% (Cd), demonstrating decreased and minimal valued in the uppermost oxidized layer at the water-bottom boundary (0–1 cm). In this layer, an exchange process between the solid and liquid phases of sediments are known to be the most intensive, which is reflected in variation of geochemically mobile fractions. Down the core, the role of the Co, Cd, Pb, and Cu lithogenic fraction was increased only slightly (Figure 14f).

## 5. Discussion

### 5.1. Lithology of the Sediment Core AMK-5194, the Central Deep of the Barents Sea

The earlier published data [3,4,18] have revealed some differences between the post-glacial shelf depression facies and the Holocene sediments in the Barents Sea. As a whole, the grain-size analysis of the sediment core AMK-5194 corresponds to published data, which indicates that sediments of the Late Deglaciation (Unit II), with absolute predominance of fine-grained clay fraction, transferred into the Holocene clayey–silt and sandy–silty–clay sediments. There was almost no coarse debris (gravel and pebbles) in sediments of Units II and I, in the latter, the very fine sand (0.1–0.05 mm) constitutes a noticeable proportion of the >0.05 mm fraction (Table S1). Thus, the Holocene sediments of Unit I are relatively coarser when comparing to Unit II, while, in the latter, sediments are composed of the extremely fine-grained clay, which is displayed in Figure 15.

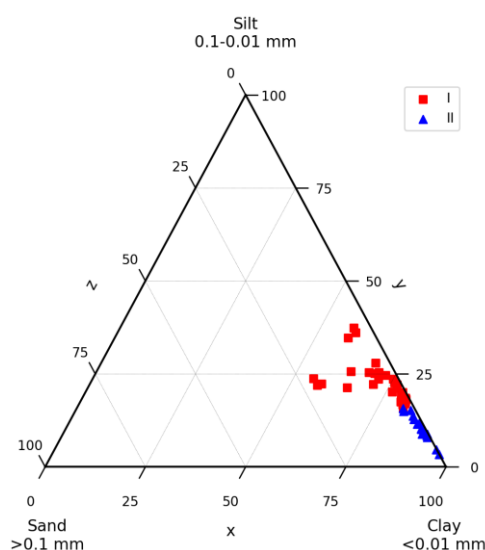


**Figure 15.** Ternary diagram of grain size composition (%) in the stratigraphical Unit I, 0–290 cm (red dots), and Unit II, 290–444 cm (blue dots) from core AMK-5194, the Central Deep of the Barents Sea.

In the bottom part of Unit I (220–290 cm), corresponding to Early Holocene, the elevated contents of silt and sand fractions (to 46% of total sediment) may suggest the deposition caused by a rather strong bottom currents from the West-Southern shelf areas. An increased supply of terrigenous material was typical of the Early Holocene sedimentation, which resulted in an increase in rates of sediment accumulation under conditions of the continued retreat of mainland glaciers and significant ice cover in the southern Central Deep [3]. The published dates suggest considerable variations in sedimentation rates during the Holocene, with maximum values (up to 74 cm/ka) being obtained for the lowermost part of the Unit I in the Central Deep [2]. Sorting ( $So > 3$ ) of the Unit I sediments was deteriorated due to the coarse-grained fractions' growth and the content of silt and sand ranged within the limits of (16.78–37.41%) and (0.78–21.2%), respectively. The Unit II (290–446 cm) sediments correspond to

the Late Deglaciation (Pleistocene). Sediments are dense and characterized by plasticity, uniformity, an absence of hydrotroilite, and bioturbation. Sediments are composed of the finest clays which were absolutely predominated (81.4–96.6%). Median diameter ranges from 0.8 to 0.9  $\mu\text{m}$ , sediment are well sorted ( $So \sim 2$ ,  $So < 2$ ). Thus, the Unit II sediment in core AMK-5194 may indicate a fine-grained nature of the post-glacial shelf depression facies [4].

In the Barents Sea sediments, the coarse sand fraction ( $>0.1\text{ mm}$ ) commonly consists of a grain-sized unsorted heterogeneous material characteristic for ice-rafted debris [3,4,16]. Thus, the low contents of coarse-grained material ( $>0.1\text{ mm}$ ) in the most part of the AMK-5194 suggest the absence or minor role of the ice- and iceberg material supplied in the southern Central Deep over the Pleistocene (Unit II), as well as Mid- and Late Holocene. The exception is the Early Holocene (220–290 cm), where sandy–silt sediments with the high sand content (to 21.2%) and elevated density values (to  $1.75\text{ g/cm}^3$ ) were recorded. That corresponds to the episodic influxes of sandy–silt material from the iceberg drift in the Early Holocene [2–4].

## 5.2. Variation in Elemental Ratios in the AMK-5194 Core (Central Deep) over the Late Glacial to Holocene Periods: Relation to Sedimentation Environment

It is assumed that various environmental factors affect the distribution of elements in the sediments. For the mostly terrigenous sediments of the Barents Sea, the major factors are supposed to be related to the grain-size composition, which depends on the topography of the seafloor and velocity of currents. The element accumulation in sediments is closely linked with mineral composition, whose proportion and distribution are influenced by regional difference in feeding provinces. Mineral indicators, such as the quartz/plagioclase ratio, in cores from the North Atlantic reflects the varying contribution of continental derived quartz versus that of basaltic plagioclase and can also be used as a proxy for the contribution of ice-rafted debris [68]. The proportion of clay minerals (kaolinite and illite) characterizes the silt and coarse silty-sand fractions in the sediments of Mendeleev Ridge [11]. The feeding provinces of the Lena, Yenisei, and Ob rivers' catchment are identified by the composition of clay and heavy minerals in the shelf sediments of the Kara and the Laptev Seas [12]. The increase in sand content and the quartz/plagioclase ratio is concurrent with decreasing log (Ti/K) ratios suggesting major changes in the provenance and transport mechanism of the sediment [10].

The Upper Holocene sediments with the oxidized uppermost layer (0–10 cm), are characterized by high and strongly variable contents of Si, Ni, V, Sr, Cr, Mn, Ba, Ti, and TOC, which exceed their contents in the deglacial deposits, which was obviously attributed to the higher primary production of the present-day waters [5,50]. The Deglacial sediments, with a noticeable sand admixture were deposited during the colder climate, when the major role in transport and sedimentation of elements belonged to the products of glacial activity and the meltwater iceberg fluxes. In these sediments, which were accumulated earlier than  $\sim 10\text{ cal. ka BP}$ , minimal variability of chemical elements was recorded due to the only aeolian source of sedimentary material at that time, while a relative enrichment in  $\text{CaCO}_3$  and Ba was attributed to authigenic precipitation [5].

Some element/Al ratio indices, such as Si/Al, Zr/Al, Ti/Al, and Al/Ca, are commonly applied as proxy of the increased content of coarse-grained fraction in sediments, since sand and silt are represented mainly by quartz, feldspar, and rutile, which are resistant to weathering. A physical erosion acts as a fundamental control in the Arctic sediment composition; during deglaciation when physical weathering dominated over chemical one, a growth of the elemental ratios Si/Al, Ti/Al, and Ti/Zr, Zr/Al was revealed [7–9]. Besides, the element/Al ratio also indicates the feeding province of the terrigenous sediments [7,10].

In core AMK-5194, the noticeable variations in selected elemental ratios can be seen in Figure 9. The Si/Fe ratio displays a distinct peak at depth of 250 cm, followed by the strong growth that started at the Unit II/Unit I boundary (depth of 290 cm) and continued till Mid Holocene (depth of 220 cm). That might be caused by the two different reasons. First, an increase in contribution of the coarse sand fractions in these intervals, indicated by the coarse-grained material, mostly composed of quartz



and resistant aluminosilicates. Second reason is the abundant meltwater inflow. In the Northeastern Atlantic, relatively higher values of Si/Fe ratios are regarded a proxy for the supply of sediments from the clay-mineral-loaded glacial meltwater in warming periods [69]. In the Barents Sea ASV-1183 core, sediments of Unit II (distal glaciomarine facies) were deposited in the main deglaciation phase, when the abundant fluxes from melting large ice sheets drained directly into the open sea [4]. Ratios Ba/Al and P/Al, commonly used as proxies of paleoproductivity, display a synchronism and weak variability throughout the core. Slight peaks of both ratios are noticed in the uppermost 0–10-cm layer, and that of P/Al, at the Unit II/Unit I boundary (Figure 9). In core ASV-1183, at the Unit II/Unit I boundary and in the overlaying sediments, TOC content exhibits increase from 0.5% to 2% due to the contribution of marine organic matter which was mostly (~80% of TOC) derived from plankton production [70].

A slight increase of Si/Al and Zr/Ca ratios, recorded in the Early Holocene thickness of 210–255 cm (Figure 9), corresponds to elevated values (5.13–21.2%) of sand fraction with admixture of gravel; these evidently correlates with increased supply of terrigenous material caused by intensive bottom currents from the West-Southern shelf areas. In core AMK-5194, the average value of Si/Al ratio (2.96) is equal (3.0) to that in core PSh-6050 of terrigenous sediments from the subarctic White Sea, the Northwestern Russia [29], their downcore distribution are also similar. Ratios Al/Ca and Ti/Ca demonstrate a coherent rhythm down the core (Figure 9), their prominent peaks are detected at several depths, one of them, at a depth of 290 cm coincides with the density peak ( $1.75 \text{ g/cm}^3$ ). It corresponds to the distribution pattern of Al/Ca ratio that showed a prominent and consistent peaks with magnetic susceptibility signal in sediment core of Hatton Bank, the NE Atlantic Ocean [71].

Ratio Ti/Al characterizes the degree of mechanical sorting of the clastic material [72]. In AMK-5194 core, the Ti/Al and Fe/Al ratios display synchronous downcore variation with the peak values near the boundary Units II/Unit I (depth of 310 cm) (Figure 9). Such a distribution character of terrigenous indicators in Holocene sediments is supported by heavy minerals' composition in core ASV-1183 [4], located in close vicinity to core AMK-5194. Heavy minerals are presented by the epidote–hornblende association with rather high zircon content (to 12% of total heavy fraction), while in the Early Holocene sediments, reduced amounts of clay minerals were found. In cores from the contourite drifts Snorri and Gloria (North Atlantic,  $60^\circ \text{ N}$ ), the Al/Si, Ti/Al, and Fe/Al ratios varied synchronously to ice-rafted debris (IRD) counts; these downcore distributions showed an opposite trend with variation of Si/Fe, Mn/Fe,  $\delta^{18}\text{O}$  values and content of  $\text{CaCO}_3$ ,  $\text{BioSiO}_2$  during MIS 1–6, thus distinguishing the glacial-interglacial periods [73]. Coincident with these tendencies, the cooling periods in the Early Holocene and Subboreal stage were characterized by the growth of Si/Al and Ti/Al ratios recorded in core PSh-6050 [29].

The elevated content of Mn, as a redox-sensitive element, was used in the sediments of the Lomonosov Ridge in the Arctic Ocean to identify anoxia conditions caused by long-term ice cover [74]. Redox conditions and post-sedimentation change in bottom sediments can be traced by Mn/Fe proxy; down the core, change in Mn/Fe ratio is caused by difference in redox kinetics of these elements: increase in Mn/Fe occurs under the oxic conditions, while suboxic condition and anoxia lead to a decrease in the Mn/Fe ratio [25,73,75–77]. In AMK-5194, the Mn/Fe ratio (0.009 on average) is almost two times less than that in UCC (0.016), which may indicate the slightly reduced condition throughout the core, and it is confirmed by findings of the rare hydrotroilite concretions in the Holocene sediments.

The average Holocene optimum was characterized by intensive inflow of the warm Atlantic waters, and the transition to the late Holocene was characterized by increased bio-productivity [2–4]. In the AMK-5194 core, a rather monotonous variation in Mn/Fe ratio was recorded, with the exception of few peaks at depths of 10 cm (oxidized layer), as well as of 115 cm, and 290 cm (Figure 9). The depths of 115 and 290 cm are recognized as the boundary between Late/Mid Holocene and Early Holocene/Late Deglaciation periods, respectively (Figure 9). At that time, the sedimentation environment changed, particularly, speed of bottom currents, which rose, leading to an enlargement of oxygen concentration in water in period, when these layers have been formed. It should be noticed that, down to the core,

Mn/Fe ratios exhibit an opposite trend to that of Si/Al, Ti/Al, and Fe/Al, that evidently supports an application of these ratios for identification of contrasting paleo-environmental conditions.

In the Central Deep, the geochemical fractions of Al, Mn, Fe, Mo, Cr, Ni, Co, Cu, Pb, and Cd were quantified with 1-cm resolution of the core AMK-5193 (Table S10, Figure 14). The absolute predominance of lithogenic fraction for Al (>95%), and its considerable percentage for Fe and Cr (to 70–80%), suggested the major role a terrigenous process in the accumulation of these elements. The redox sensitive Mn and Mo demonstrated a strong geochemical mobility under the changing environment conditions; totaling portions of their exchangeable and associated authigenic oxyhydroxides fractions reached up 75% of each total content. For Cu, the highest proportion of fraction bound to organic matter was determined (Figure 14f). The downcore distribution of Pb, Cd, and Co is related to variation of the Fe-Mn authigenic oxyhydroxides' fraction. In the upper 4-cm layer, the sharp growth of this fraction and corresponding Mn/Fe ratio was detected, which confirm an application of Mn/Fe ratio as geochemical indicators of diagenetic processes. From the mean sedimentation rate (0.7 mm/year) in sediments from the Central Deep [78], core AMK-5193 (length of 37 cm) was deposited over 500 years. The upper 8-cm sediment layer was formed during the last ~100 years, when the industrial load of the mining industry on the basin increased. This seems to have affected the peaks in the total content of heavy metals due to an increase in the proportion of their geochemically mobile forms in this layer. Some features that have been revealed in the chemical elements' behavior in recent sediments of the Barents Sea are also characteristic for the recent [25] and more ancient [29] deposits of the subpolar White Sea (Northwestern Russia).

### 5.3. Elemental Distribution in the Surface Sediments

Over the entire Barents Sea, the major role in supply of fine-grained sedimentary material belongs to the Shokalsky Glacier, in the Novaya Zemlya Archipelago. The system of the Barents Sea currents has a semi-closed cyclonic character, so the fine-grained material was likely not carried outside the shelf area [44]. The distribution of sediment fractions over the seafloor are characterized by the vertical and circum-continental zonality: sands are common in shallow areas or near the coasts, deeper and further from the shelf, proportions of the coarse fractions are reduced, while that of fine-grained material, in contrast, are increased [79,80].

The spatial distribution of the potentially toxic heavy metals in surface sediments over the last twenty years was studied in detail [21]. As a regional background, these authors used the scale of the Norwegian state Agency for environmental pollution control for the coastal area of the Norwegian Sea [81]. In the clay sediments of the Western Barents Sea, Central Deep and Trough, coastal sediments of the Southwestern areas, the Western part of the Novaya Zemlya Trough, the considerable increase (to two-fold) of Ni, Cu, Zn, and Pb contents, as compared to background was detected. Spatial distribution of Cr, Ni, Cu, Zn, Cd, and Pb in surface sediment is controlled by mostly the global geochemical background, also in sediments near the Shtockman gas-condensate field and in the Cambridge Strait, elevated contents of Ni and Cu were detected [82].

Our data on surface sediments revealed the elevated (20 to 60%) Cr, Ni, and Co concentrations when comparing to the regional background values. These may suggest an evident relation to the ore mining and processing the cobalt-nickel enterprises located on the Kola Peninsula, such as the Severonikel and Pechenganikel. At the same time, high As content, which is two times more than that in the UCC, should not allow considering these sediments as contaminated, since there are no data on the regional background values. It is assumed that As is supplied from peat and sedimentary rocks bearing coal inland. The coal and coal pits have high As contents [83,84].

The larger part of the Kola Transect belongs to a wide continental shelf, where the distribution of sediments is strongly influenced by the different currents (Figure 1). Our data on elemental contents in sediments of the Kola Transect allow to consider some aspects of spatial distribution patterns in rather contrasting environments, caused primary by differences in grain-size composition. It should be noticed that the distribution pattern of elements is not always continuous. Elemental ratios seem to

heighten a relationship between contents of elements and grain size composition. Our data showed that a rather strong correlation ( $R^2$  0.69) exists between lg Md and Si/Al, which is used as a proxy of coarse-grained fractions. A coherent distribution of the Si, Ba, and Zr contents and percentage of coarse-grained fractions (Figures 4 and 8) was revealed. In the coarse-grained (essentially siliceous) material, Zr is mainly accumulated with peak content of 209 ppm, detected in sediments of st. 5554 with maximum gravel content. In the southern part of Kola Transect (st. AMK-5548, -5578, and 5579), influenced by the Atlantic-Norwegian and North Cape Currents, distribution of Ca and, in to a lesser degree, of Sr is mostly related to the sandy–silt fraction of sediments, where the remains of calcareous fauna are commonly found. A similar distribution was revealed in surface sediments near the Japanese Islands, where high Ca and Sr contents were found in shallow areas with large amounts of calcareous shells and foraminifera [85]. A few tendencies can be seen from the elemental ratios' distribution. A prominent peaks of Si/Al ratio, and, to a less extent, that of Ba/Al and Si/Fe, were detected in AMK-5578 station (Figure 16a), which corresponds to maximal content of sand fraction (53%) (Figure 4). Peak values of Zr/Ca and Al/Ca ratios, found at AMK-5554 station, might be related to maximal content of gravel (to 24%) in sediment. In the distribution of Al/Ca and, particularly, Mn/Fe ratios, a significant decrease from the Northern to Southern part of the Kola Transect was revealed (Figure 16b,c). In the shallow southern part of the Kola transect (sts. AMK-5578, -5579) with increased contents of silt and sand fractions, a prominent decrease in Al/Ca ratio is evidently caused by a significant growth of the Ca content: from 0.73% in the northern part (AMK-5556), to 1.45% in the southern ones (AMK-5579). In contrast, Mn shows a decrease from the northern part of transect to the southern one, which may be explained by two reasons. Firstly, that might be caused by a predominant Mn accumulation in the fine-grained clay fraction, whose content reduced from the North to the South.

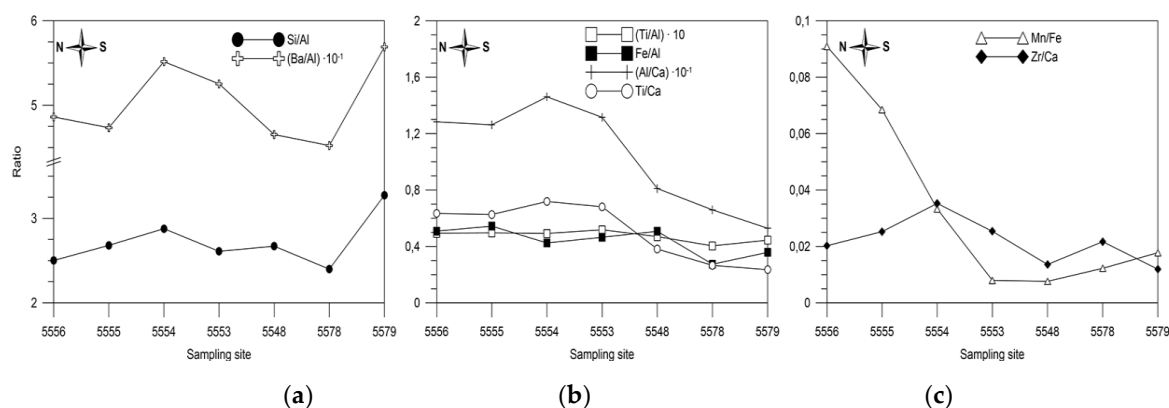


**Figure 16.** Variation of elemental ratios in surface sediments at the Kola Transect along the 32.400° E, the Barents Sea: (a) Si/Fe, Ba/Al; (b) Ti/Al, Fe/Al, Al/Ca, Ti/Ca; and, (c) Mn/Fe, Zr/Ca.

Secondly, in the Northern part of the Kola Transect, the elevated content of Mn in sediments may result from increased content of this important micronutrient in suspended particulate matter that is produced by increased biological productivity in the Polar Front water mass, which migrates nearby there. Southward, a general, although a rather irregular, trend to increase in coarse-grained fractions' (sand and gravel) was detected. The Fe/Al, Ti/Ca, Zr/Ca, and Ti/Al ratios exhibited a rather smooth profile (Figure 16b,c), which could be related to a rather irregular distribution of the grain-size fractions percentage along the Kola Transect.

It should be noticed that the distribution pattern of elements is not always continuous. A contrasting behavior of different elements was revealed: Si, Zr, and Ba display a coherent distribution pattern with the coarse sand fraction, while Ca and Mn proved to be the most sensitive elements to change in the proportion of silt and clay fractions correspondingly.

#### 5.4. Radionuclides' Distribution in the Modern Sediments

##### 5.4.1. Sources of Artificial Radioactivity in the Barents Sea

The main source of artificial radionuclides in the oceans is the nuclear weapons tests. During about half a last century, more than 2500 nuclear explosions were conducted. Their total yield was 440 Mt, including 160 Mt due to fission. Approximately 90% of the tests were conducted in the Northern hemisphere. The residence time of aerosols in the stratosphere can be as long as two to three years, and even five to ten years in cases where aerosols have reached great heights, about 100 km [86]. The tropospheric component precipitates to the ground locally or within the region, whereas the stratospheric component is predominantly distributed within a hemisphere. The maximum fallout of radionuclides was at the latitudes 30–50° in both hemispheres. The maximum of atmospheric deposition corresponds to 1963 (Figure 17). One of the most significant products of nuclear explosions is Cs-137. Americium-241 does not arise in explosions, but it is generated during the radioactive decay of plutonium-241 ( $T_{1/2} = 14.35$  years).

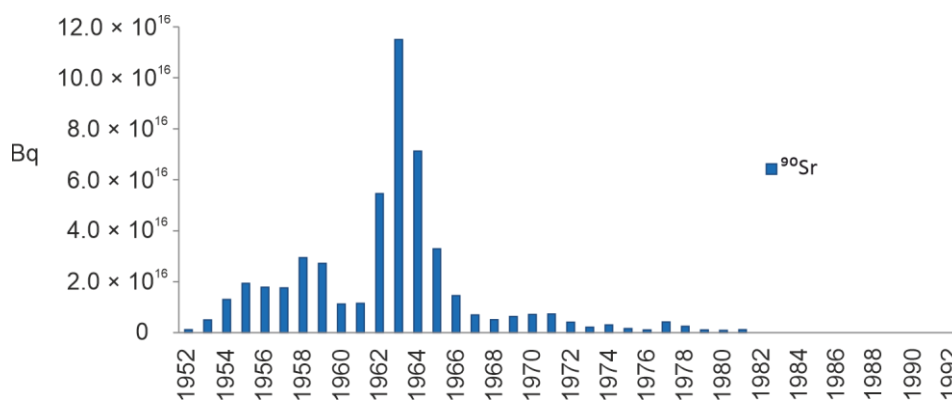


Figure 17. Annual Northern hemispheric  $^{90}\text{Sr}$  fallouts (calculated) [87].

The nuclear fuel reprocessing facility in the Sellafield has been discharging the liquid radioactive waste to the Irish Sea since the early 1950s. The maximum  $^{137}\text{Cs}$  discharge was observed in 1975 (about 5.7 PBq). The discharge then gradually decreased, stopping almost completely in 1986. The maximum releases of  $^{241}\text{Pu}$  occurred around 1973 (Figure 18).

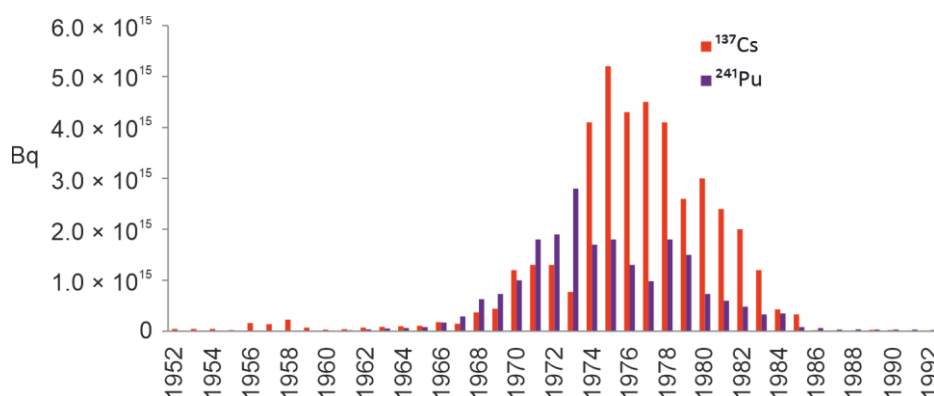


Figure 18.  $^{137}\text{Cs}$  and  $^{241}\text{Pu}$  discharges into the Irish Sea [88].

The results of measurements of the surface water radioactivity in the southwestern part of the Barents Sea (71°–72° N, 20°–30° E) from the early 1960s to 1990 are reported [89]. The highest activity of  $^{137}\text{Cs}$  was observed in the first half of the 1980s, which corresponds to a transit time from Sellafield to the Barents Sea of 4–5 years. Later estimations were done using  $^{99}\text{Tc}$ ; they turned out to

be close and amounted to  $42 \pm 9$  months [90]. Plutonium behaves less conservatively in the marine environment than caesium and technetium. However, despite this fact, plutonium discharges from the Sellafield were traced at a significant distance from the source. The  $^{238}\text{Pu}/^{239} + ^{240}\text{Pu}$  ratio in discharge significantly differs from corresponding value for global fallout and, therefore, may be used as a reliable marker of discharges. This made it possible to trace plutonium in a dissolved fraction of surface waters of the North Sea and Norwegian Current in 1981 and then at a distance up to 2500 km from the source [89]. The relative mobility of plutonium in surface waters can be explained by the fact that it is mainly present in the form of a single-charged cation  $\text{PuO}_2^+$  [91,92]. Direct discharges of americium also took place, but this radionuclide is more particle-reactive than plutonium and caesium, and it is unlikely to migrate over long distances. Zaborska et al. [93] noted that 19–27% of plutonium in the North-West of the Barents Sea originates from sources other than global fallouts, probably from Sellafield. The accident in Chernobyl NPP in 1986 becomes another possible source of  $^{137}\text{Cs}$  in the Arctic marine environment [94]. The long-distance transfer of actinides during the accident did not occur.

#### 5.4.2. The $^{210}\text{Pb}$ and Sedimentation Rates in the Barents Sea

Sedimentation rates were previously determined for the western part of the Barents Sea [78]. They varied over a fairly wide range—from 0.3 to 1.3 mm per year (average value of 0.7 mm per year). The sedimentation rates, obtained in this study for the western Barents Sea (AMK-5432 core), are also within these limits. The rate of sediment accumulation in the Cambridge Strait is much higher, possibly due to the proximity of land and suspended matter's supply from the Franz Josef Archipelago. We failed to determine the rate of sedimentation in core AMK-5424, sampled in the Russkaya Gavan' Bay. This is due to the fact that the glacier's discharge from the Novaya Zemlya Land Archipelago strongly reinforces sedimentation of suspended matter, which occurs at a very high rate. As a result, only the upper portion of the sediment core deposited over the anthropogenic time-scale, was sampled by MUC. According to the distribution of caesium-137, we can only give a lower estimate of the sedimentation rate, 4 mm per year; further studies are needed for a more accurate determination. The high sedimentation rate also is confirmed by the uniform distribution of lead-210 and the low specific activity of  $^{137}\text{Cs}$  in the sediment core.

#### 5.4.3. The Artificial Radionuclides in the Barents Sea

The content of caesium-137 in the Barents Sea sediments was investigated in the number of works. Most often, they focused on the surface layer of sediments. Specific activities of caesium-137 in the surface layer of bottom sediments taken in the northern and western parts of the sea in 2007–2009 amounted to 0.3–6.2 Bq/kg [95]. In the same period, another study was conducted in the central, northern, and western parts of the water area with approximately the same results [96]. Similar values are given in the work of Matishov et al. [97] for sediments that were sampled in 2001–2007 in various locations of the Barents Sea, including stations near the Franz Josef Land and Novaya Zemlya archipelagos. The same order of magnitude was obtained in this work. The vertical profiles of caesium-137 were studied in [92]; according to the results, it was concluded that the sediments were mixed.

The presence of americium-241 in sediments is a particular feature of these sediment cores. The maximum of its activity in 5454 is located on the horizon of 7–8 cm. This radionuclide is a decay product of  $^{241}\text{Pu}$ . Americium is tightly bound to suspended matter. Pu and Am are both absent in the Chernobyl debris, but  $^{241}\text{Pu}$  presents in the global fallout and in the discharges of reprocessing facilities. Because caesium-137 is observed much deeper in the core, it is unlikely that the maximum of americium in the horizon 7–8 cm can be attributed to global fallout. If we assume that it originates from Sellafield, then a horizon of 7–8 cm can be attributed to the year ~1982, based on a transit time of ~5 years. The second small maximum in the horizon of 12–13 cm can then be attributed to the global fallout of 1963. Two  $^{241}\text{Am}$  maxima were also found in the core AMK-5432. The deeper peak



may be attributed to 1963, which is in good agreement with lead-210 age-dating. The position of the upper maximum of americium-241 (presumably 1982), gives an almost twice lower sedimentation rate. However, due to poor time resolution, small inaccuracies in determining the depth of the horizon, in this case, can lead to large errors in the estimation of the sedimentation rate.

Generally, there is a good agreement between the vertical profiles in cores AMK-5432 and 5454 of artificial radionuclides and sedimentation rates derived from lead-210. A comparison of different approaches to age-dating of the core is given in Figure 19.

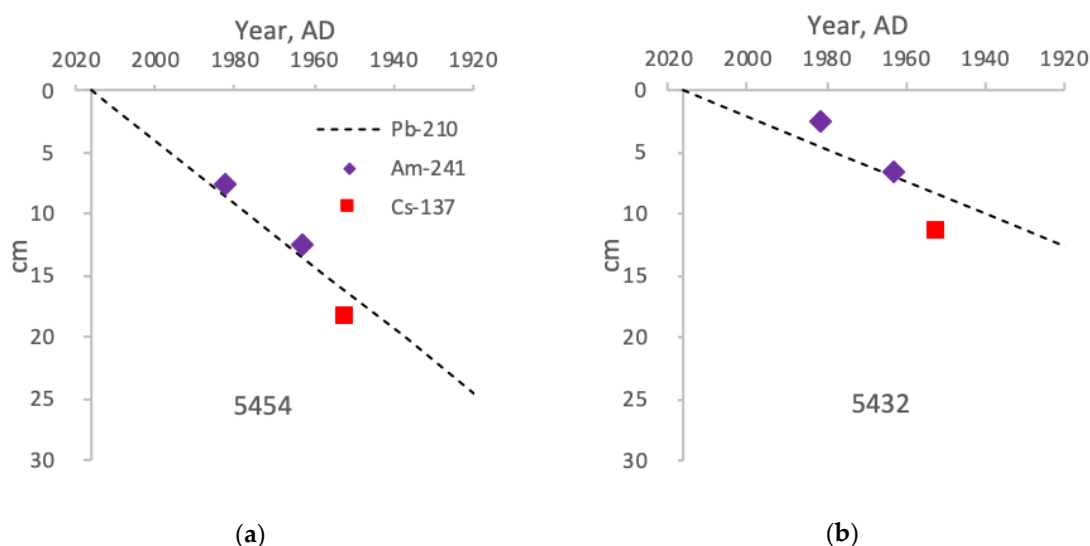


**Figure 19.** An age model constructed using excess lead-210 and its correspondence to chronostratigraphic markers  $^{241}\text{Am}$  and  $^{137}\text{Cs}$  for the sediment cores AMK-5454 (a), the Cambridge Strait, and AMK-5432 (b), the Bear Island Trough.

### 5.5. Mineral Composition of the Modern Sediments in the Barents Sea

As a whole, the wide range of minerals, totaling over 25 mineral species, was identified. The mineral complexes of clastic minerals varied from 41% to 79%, while clay mineral totaling from 21% to 59% of bulk sediment. The four mineral associations groups could be distinguished: (i) terrigenous detrital minerals, which included a different proportion of quartz (12–49%), potassium feldspar (3–14%), albite (9–23%), anortite, andesine, labradorite (4–42%), and amphibole (2–4%), pyroxene (1–11%), muscovite (6–15%), epidote (1–4%); (ii) clay minerals were constituted by illite (5–18%), kaolinite (1–14%), chlorite (2–48%), smectite (1–18%), and mixed-layered forms; (iii) carbonate minerals were presented by calcite (4–7%), dolomite (1–2%), aragonite (1–2%); and, (iv) authigenic minerals had a strongly subordinated contents: gypsum (1–2%), zeolites (1–7%), and pyrite (traces). The diffraction characteristics of registered zeolites (Mordenite, Ca-Heulandite, Clinoptilolite) correspond to the Ca-forms of these minerals, wherein the structural positions of freely bound cations are mainly filled with the  $\text{Ca}^{2+}$  cations supplied to the bottom waters as a result of basalt epigenesis.

One of the results of this work is the identification of contrasting mineral clay complexes (Figure 20), which, along with the clastic components, can be used to identify the mineralogical provinces of the basin and further reconstructions of the paleo-environmental conditions.

The diversity of clay mineral complexes in the surface sediments of the Barents Sea is recognized in both the qualitative composition and quantitative proportion. These features determine the sorption properties of bottom sediments, together with the clastic components they may impact the geochemical characteristics. The diagnosed complexes of clay minerals in combination with clastic components clearly indicate the sources of mineral material. At the stations 5454 and 5452, as well as 5424, sediments are marked with mineral matter supplied by the Franz Josef Land and Novaya Zemlya Archipelagos, respectively (Figure 21). The Western edges of the Barents Sea are influenced by the North Atlantic

currents. The characteristic feature of sediments in the Bear Island Trough (AMK-5432) is a noticeable amount of calcite (to 7%). As a result, the relative content of the clay minerals, which in the upper layers varies from 21% to 35%, is reduced. Here, illite is the dominant mineral, while smectite was commonly not recorded in some samples.

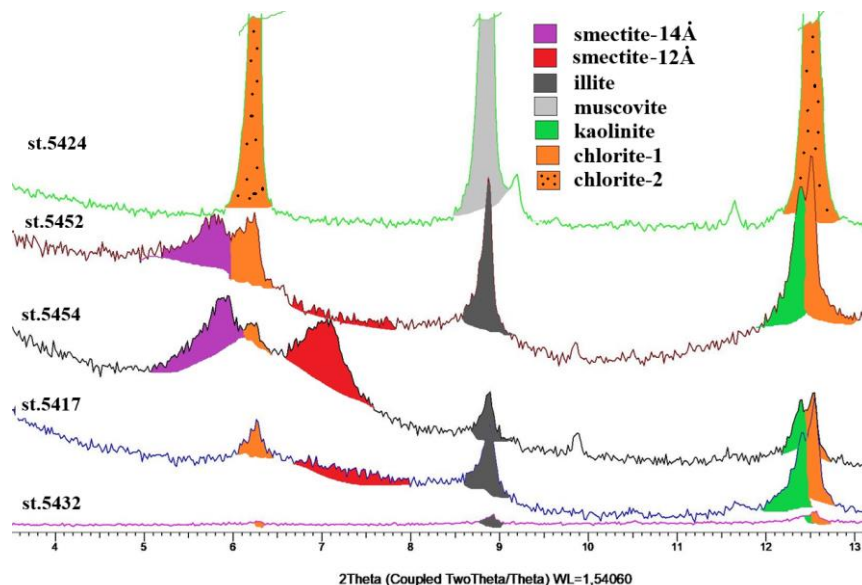


**Figure 20.** X-Ray diffractograms' fragments (small-angle diffraction) of surface sediments (0–1 cm) from different areas of the Barents Sea: st. 5432—the Bear Island Through; st. 5417—the Central Deep, the Shtockman field; st. 5454—the Cambridge Strait, the Frans Josef Land Archipelago, st. 5452—the most northern core, Kola Transect; st. 5424—the Russkaya Gavan' Bay, the Novaya Zemlya Archipelago.

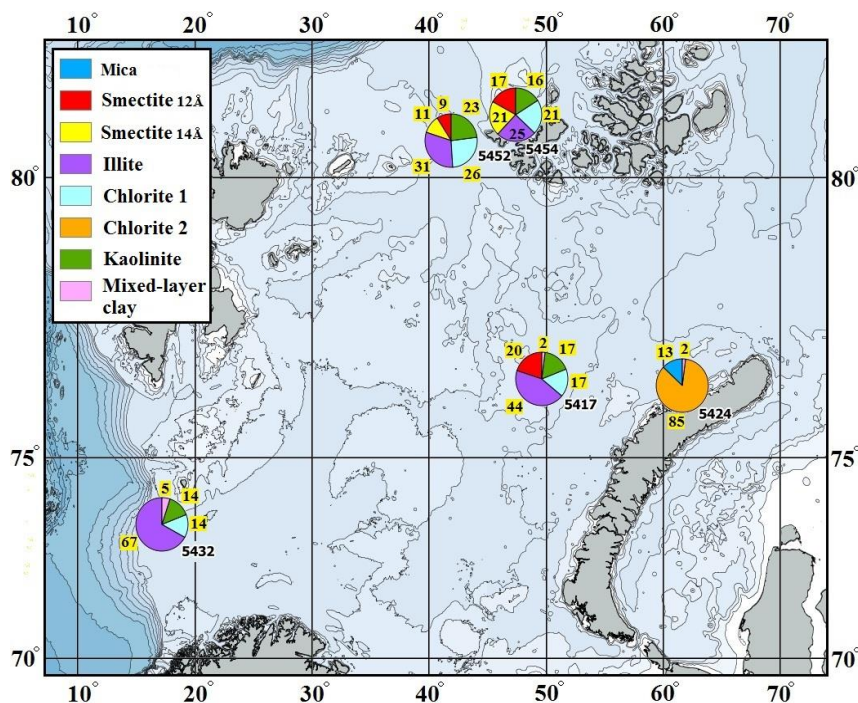


**Figure 21.** Diversity of clay mineral in the surface bottom sediments of the Barents Sea, in accordance with the cores studied: 5432, 5452, 5454, 5417, and 5424. Values around the circle diagrams indicate percentage of minerals.

Mineral analysis of bottom sediments in the area near the center of the Barents Sea (st. 5417) did not yield mineral markers, typical for the marginal seas. These sediment does not contain mineral markers that are characteristic of sediments described above, such as carbonates (st. 5432), basic plagioclases and alkaline earth smectite (st. 5454), sericite, well-crystallized micas, and chlorite (st. 5424). In core AMK-5417, the mineral composition is generally typical for the central regions of the Arctic Seas, remote from the continent, and archipelagos. There are as follows: quartz; albite (the most resistant of plagioclases to degradation); potassium feldspar (microcline); small portions of (to a few %) amphiboles and pyroxenes; and, 12.5-Angstrom smectite. The latter was the single mineral from this group. In addition, there are the Mg-Fe chlorite, kaolinite, and illite; the latter is predominant mineral among the clays (Figure 21).

The highest sorption capacity is characteristic for clay minerals that compose large portion of bottom sediments of the Cambridge Strait (st. 5454): clay mineral content in bulk sediment reaches up to 47%. Among clay minerals, smectite was found in noticeable quantities (to 18% of bulk sediment). The clastic components are represented by the basalt complex minerals; the basic plagioclases, pyroxenes. The low value of the quartz-feldspar ratio  $Q/Fps$  (0.4–1.2) indicates a reduced contribution of continental material (Figure 22a).

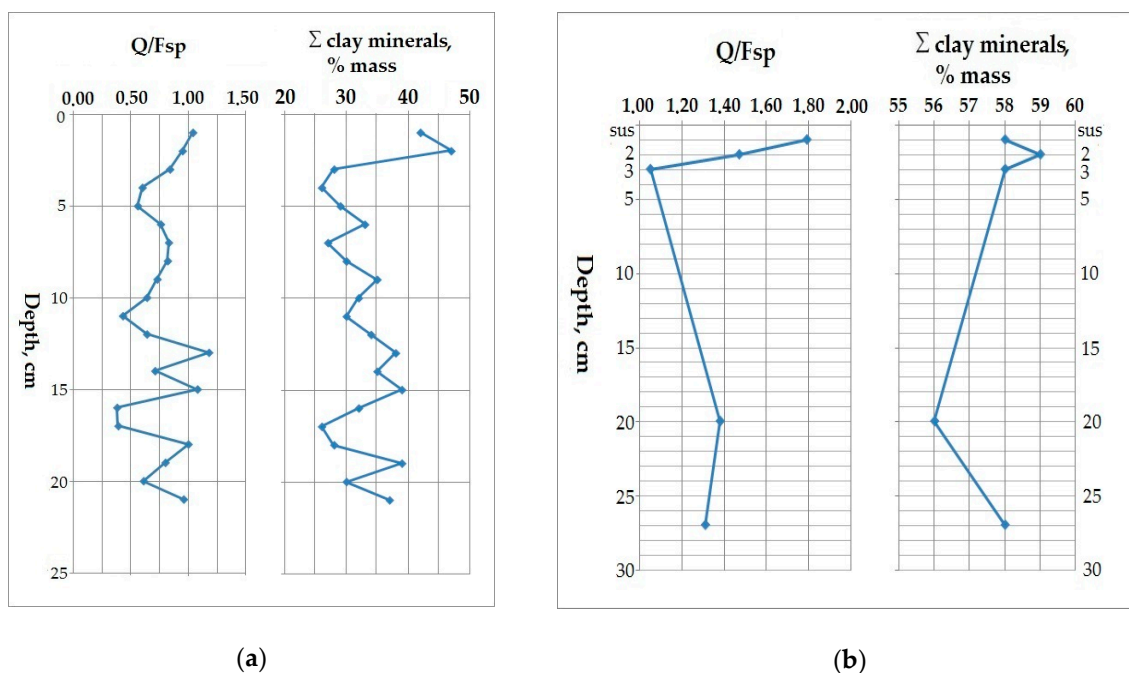


**Figure 22.** Downcore change in the quartz-feldspar ratio ( $Q/Fsp$ ) and total content of minerals of the clay group in the AMK-5454 core, the Cambridge Strait, Franz Josef Land (a), and in the AMK-5424 core, the Russkaya Gavan' Bay, the Novaya Zemlya Archipelago (b).

The major minerals of the clay group in sediments of the Russkaya Gavan' Bay (st. AMK-5424, the Novaya Zemlya Archipelago) are chlorite and the 10-Angstrom minerals that are represented by muscovite, sericite, and illite. The total content of the clay minerals varies between 56% and 59%. The almost invariable proportion between minerals is seen throughout the core length of 24 cm (Figure 22b). The uniformity of the mineral composition, characteristics of minerals of the clay fraction, and values of the quartz-feldspar ratio  $Q/Fps$  (1.05–1.79) over the entire depth of the column indicate that the sedimentation environment and material source were evidently invariable during this period.

### 5.6. Comparison of Elemental Ratios' Distribution in Different Sedimentation Environments

As it was mentioned above, the most active hydrodynamics conditions were observed at st. AMK-5432 (the Bear Island Trough), located at the western border of the Barents Sea, while more calm sedimentation environments are characteristic for core AMK-5424 (Russkaya Gavan' Bay) and AMK-5454 (Cambridge Strait). The rates of sedimentation, according to our  $^{210}\text{Pb}$ -based age model, are also different in those three cores. The highest one, amounting  $> 4$  (to 13) mm/year, was determined in core AMK-5424, Russkaya Gavan' Bay, Novaya Zemlya Archipelago, which was obviously caused by abundant meltwater discharge of the Shokalsky Glacier ("glacier milk"). In AMK-5454 (Cambridge Strait, Franz Josef Archipelago), the sediments were deposited with the sedimentation rate of 2.5 mm/year, while in core AMK-5432 (Bear Island Trough) sedimentation rate was much lower, 1.8 mm/year. Assuming the constant rates in each core studied and based on mean sedimentation rate, a time-scale of sediment deposition can be estimated as no less that 60 years (27-cm core length AMK-5424, 115 years (33-cm core length of AMK-5454), and 140 years (25-cm core length of AMK-5432).

A present-date sedimentation environment in different part of the Barents Sea seems to influence differences in grain-size composition of the cores studied, which, along with the mineral composition, influence the chemical composition and elemental ratios' distribution. Comparison of the downcore variation of grain-size fractions in the AMK-5424, AMK-5432, and AMK-5454 is displayed in Figure 23.

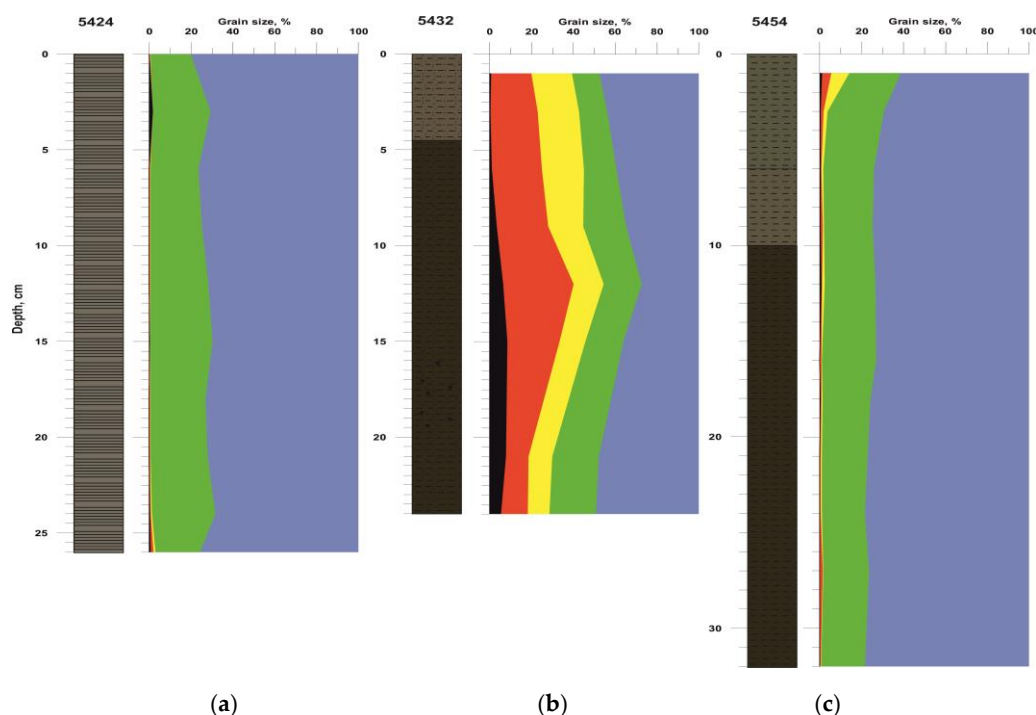


**Figure 23.** Lithology and grain-size distribution in the modern sediments cores, AMK-5424 (a), AMK-5432 (b), and AMK-5454 (c). For symbols, see Figure 2.

The cores AMK-5424 (the Russkaya Gavan' Bay) and AMK-5454 (the Cambridge Strait) are similar in proportion of the fine- and coarse-grained fractions: predominance (60–80%) of the clay fraction with a subordinate silt content and insignificant coarse-grained fraction ( $>0.1$  mm) total sediment. In core AMK-5454, the clay fraction varied from 73% to 92%, with ~50% of the finest ( $<0.001$  mm) particles (Table S2). In both cores, such a rather monotonous downcore grain-size distribution (Figure 23a,c) corresponds to a uniform supply of terrigenous material over the sampled intervals. Unlike these, core AMK-5432 is characterized by the high content of coarse-grained (ranged from  $>0.1$  to  $>1$  mm) fractions, totaling up to 40% in the middle part of the core (Figure 23b).



In the Russkaya Gavan' Bay (AMK-5424), the absolute predominance of pelite-size material (~80%) is reflected in dominating clay minerals: highly ordered Fe-chlorite (43%), illite+muscovite (15%), while quartz has a strongly subordinate proportion (22%). Mineral complex showed a homogeneous downcore variation. The stability of sedimentation environment and the material source related with the sedimentary rocks phyllites, clay, and crystalline shales of the Northern Novaya Zemlya Archipelago is supported by elevated values of the quartz-feldspar ratio Q/Fps (1.05–1.79) throughout the core AMK-5424 (Figure 22b). The downcore uniformity of elemental composition is reflected in the invariable values of Si/Al, Mn/Fe, P/Al, and Ti/K ratios in core AMK-5424 (Figure 24).

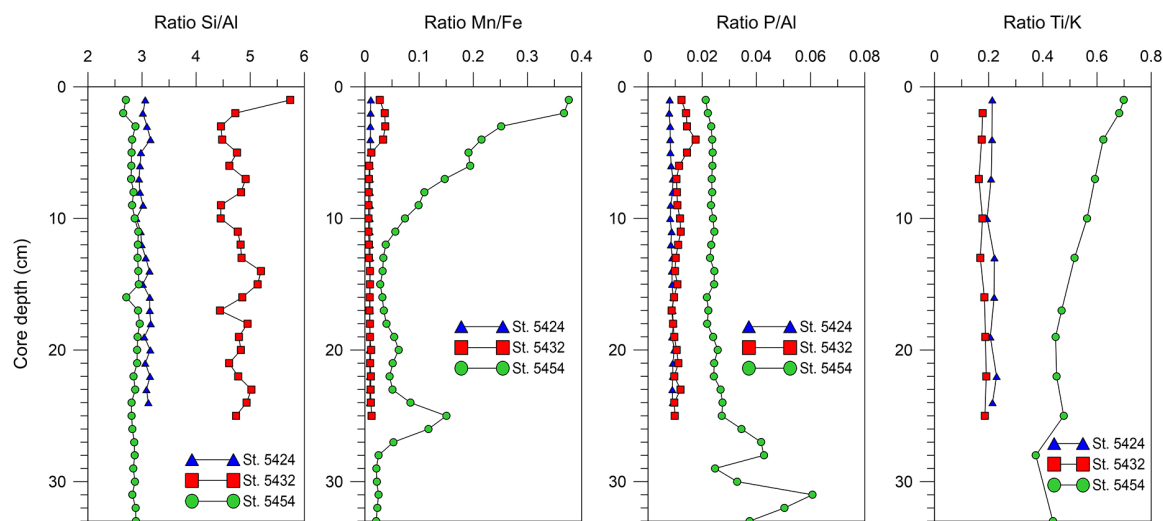


**Figure 24.** Comparison of selected elemental ratios in sediment cores, formed under different environmental conditions: AMK-5424, the Novaya Zemlya Archipelago; AMK-5432, the Bear Island Trough, and AMK-5454, the Franz Josef Land Archipelago. (a) Si/Al; (b) Mn/Fe; (c) P/Al; (d) Ti/K.

Sediments in the Bear Island Trough (AMK-5432) with an increased proportion of coarse-grained material (to 46%) are distinguished by the high percentage of clastic minerals, totaling about 70%, and the presence of calcite (to 7%). Among clastic minerals, quartz, feldspar, minerals of the amphibole, and pyroxene groups dominated, which are associated with the sand and gravel fractions. The contents of clay minerals, with prevailing illite (to 35%), are lower than in other areas of the Barents Sea. In AMK-5432 core, along with much higher contents of Si (30.37%) and Zr (230 ppm) and the low Al (6.33%) mean contents, as comparing to AMK-5424, -5454, and UCC, were registered (Table 3). The downcore distribution of Si/Al ratio exhibits a clear rhythmic variation: four higher values are alternating with four lowered ones (Figure 24a). The maximal Si/Al value in the uppermost layer might indicate the presence of biogenous matter produced by diatoms in this part of the core. The values of Zr/Al ratio display the similar distribution pattern (Table S6). Such downcore variations in Si/Al ratio, which serve as a grain-size proxy, may suggest change of deep-water dynamics during the sediment deposition.

In core AMK-5454, the high mean contents of Fe (8.87%), Mn (0.793%), (Ti (0.71%), and P (0.21%), as well as considerably higher ratios of Fe/Al (1.20), Ti/Al (0.09), Mn/Fe (0.09), Ti/K (0.51), and P/Al (0.03), when comparing to that of UCC (Table 3), point to a significant contribution of the watershed basalts' weathering products, associated with trap magmatism, into sediment composition of the Cambridge Strait, Franz Josef Land Archipelago. These correspond to the mineral association of clastic components, as presented by the basaltic complex of minerals, such as the mafic plagioclases and pyroxenes. The low value of the quartz-feldspar ratio Q/Fps (0.4–1.2) (Figure 22a) may indicate an insignificant supply of the continental material and enlarged contribution of the weathered basaltic rocks. On the other hand, the predominance of pelite-size material with large percentage of fine-grained fraction (<0.001 mm), as well as increased Fe, Mn, Zn, and Cu contents, reflect the substantial contribution of clay material



derived from glaciers' meltwater fluxes. The clay minerals (smectite, hydromuscovite, kaolinite, and chlorite), totaling 26% to 47% down the core, are characterized by the highest sorption capacity. The high Mn content (0.793% on average) in core AMK-5454, is consistent with the data [19] for the Northeastern part of the Barents Sea. The additional possible reason for it, related with increased primary productivity in water mass of the Polar Front, is mentioned above. It should be noticed that core AMK-5454 was sampled in the northernmost area ( $\sim 80.593^\circ$  N) with the longest ice-covered period, when hypoxia may be developed. It could promote a reducing condition, which led to a change in redox conditions, followed by the diagenetic redistribution of elements. The Mn/Fe ratios display a growth in the upper 0–7 cm layer (Figure 24b), which reflects the oxidation of Mn (II), diffused from underlying suboxic-reduced sediments, where the authigenic hydrotroilite and organic remains were found, indicating the early diagenetic processes.

The highest sedimentation rates were determined in the Russkaya Gavan' Bay, where the deposition was the most intense. It resulted in weak mechanical and geochemical differentiation reflected in the almost invariable mineral composition, as well as Si/Al, Mn/Fe, P/Al, and Ti/K ratios down the core. The sediments of the Bear Island Trough with the minimal sedimentation rate and strongly elevated coarse-grained fraction, in contrast, are characteristic by the much higher Si/Al indices and a few prominent peaks, showing rhythmic variation, along with the weak change in the Mn/Fe, P/Al, and Ti/K ratios down the core. Unlike these, in the Cambridge Strait, sediments exhibit the strongly elevated values of Mn/Fe, P/Al, and Ti/K ratios and the noticeable downcore variation (Figure 24b–d). In the AMK-5454 core (Cambridge Strait), a reduced contribution of continental material was detected; clay minerals compose up to 47% of bulk sediments, with considerable amounts of basic plagioclases and pyroxenes. In this core, the mean elemental ratios Fe/Al, Ti/Al, Ti/K, and P/Al are 1.5 to three times, and Mn/Fe is 10 times more when comparing to those in AMK-5424 (Russkaya Gavan' Bay) (Table 7). Those might suggest that an average composition of core AMK-5454, the Franz Josef Land, is similar to that of average deep-sea clays, however in the latter, the sedimentation rates are strongly reduced. In contrast, Si/Fe ratio in AMK-5424 core, the Novaya Zemlya Archipelago, is almost three times more than that in AMK-5454. These differences might be caused by different mineral composition, as well as different sources of sedimentary material.

Thus, the considerable differences in sedimentation environment in these three cores have been recognized by applying such paleoenvironmental proxies as mineral indicators and elemental ratios.

## 6. Conclusions

The presented data allowed to make the following conclusions:

(1) For the first time, concentrations of the artificial radionuclides and sedimentation rates were determined in the recent sediments of the Bear Island Trough, the Cambridge Strait (Franz Josef Land), and Russkaya Gavan' Bay (Novaya Zemlya Archipelago). The concentration of  $^{137}\text{Cs}$  in sediments is low, and it does not exceed 10 Bq/kg, which corresponds to the regional background values. The highest activity levels were found near the Franz Josef Land. Moreover, the samples contain appreciable amounts of  $^{241}\text{Am}$ , up to 2.6 Bq/kg. The highest sedimentation rates were found in Russkaya Gavan' Bay ( $>4$  mm/year), while slightly lower ones, in the Cambridge Strait (2.5 mm/year). In the western part of the Barents Sea, the sedimentation rate is much lower (1.3 mm/year).

(2) The relationship of mineral complexes with the main supply sources was noted, and the scale of their distribution was shown, to a first approximation. For the Northern and Northwestern areas, the main mineral markers are plagioclases, clinopyroxenes, and alkaline earth smectite, which are genetically associated with the Franz Josef Land basalts. The western border of the Barents Sea (the Bear Island Trough), which is influenced by water mass inflow from the Atlantic Ocean, is characterized by a low clay content and the presence of carbonates, mainly biogenic calcite. For sediments of the Eastern part of the Sea (the Novaya Zemlya Archipelago), a combination of high chlorite content with group of 10-angstrom minerals (muscovite, sericite, illite) is indicative. All of these minerals have a highly organized crystalline structure that is not damaged in the multi-stage sedimentation process,

which is distinctly reflected in the diffraction profiles. According to XRD data, in the central part of the Barents Sea, the influence of sediment sources described above is minimal. Each mineral complex, as mentioned above, has a characteristic diffraction profile, which allows for differentiating bottom sediments for further paleoreconstructions. However, first of all, the geochemical characteristics of the region are naturally related to the variety of mineral complexes and they are marked with structurally typomorphic features of the minerals included.

(3) Some elemental and mineral proxies for recognizing change in the environmental conditions were tested in the above-mentioned three sediments cores of the recent sediments (to 33 cm length), whose age did not exceed 140 years. Along with the mean sedimentation rates, these sediments differ in grain-size and mineral composition, as well as elemental contents. These characteristics are obviously related to a different sediment source: the basaltic province associated with trap magmatism of the Franz Josef Land, and the sedimentary rocks (phyllites, clay and crystalline shales) of the Novaya Zemlya Archipelago, while sediments from the Bear Island Trough are deposited under unstable conditions of bottom currents bearing sedimentary material from both the Atlantic and Arctic oceans. The most intense sediment deposition in the Russkaya Gavan' Bay is reflected in the highest sedimentation rates, leading to weak mechanical and geochemical differentiation. As a result, throughout the core of the Novaya Zemlya Archipelago, mineral composition, as well as values of Si/Al, Mn/Fe, P/Al, and Ti/K ratios, are lowered and almost invariable, accompanied by elevated values of the quartz-feldspar Q/Fps ratio (1.05–1.79). The sediments of the Bear Island Trough with the minimal sedimentation rate and strongly elevated coarse-grained fraction, in contrast, are characteristic by the much higher Si/Al indices, showing rhythmic variation, along with the weak change in Mn/Fe, P/Al, and Ti/K ratios down the core. Unlike these, in the Cambridge Strait, the low value of the quartz-feldspar ratio Q/Fps (0.4–1.2), along with the lowered Si/Al and strongly elevated Mn/Fe, P/Al, and Ti/K ratios, indicate an insignificant supply of the continental material and enlarged contribution of the weathered basaltic rocks. Besides, the downcore distribution pattern of Mn/Fe, P/Al, and Ti/K ratios differs from that in the Bear Island Trough and Russkaya Gavan' Bay. For this reason, these three ratios have been proposed as good proxies for detecting the differences in the short-term change in sedimentation environment.

(4) At the millennial scale, the sedimentation paleo-environmental changes were more pronounced, and they reflected in sediment record. In the Early Holocene thickness, as well at the boundary Early Holocene/Late Deglaciation periods (core AMK-5194), an increased supply of terrigenous material that was linked with the intensive bottom currents from the West-Southern shelf areas was marked by increase in Si/Al and Zr/Ca ratios. The distinct growth of Si/Fe ratio within the thickness of 220–290 cm, deposited from the Unit II/Unit I boundary (depth of 290 cm) until Mid Holocene (depth of 220 cm) may be caused by the two different reasons. First, an increase in the contribution of the coarse sand material (21.2%) in this interval, mostly composed of quartz and resistant aluminum silicates. Second, it could be resulted from the abundant fluxes of clay-mineral-loaded glacial meltwater, during the main deglaciation phase. Ratios Ba/Al and P/Al, applied as paleo-productivity proxies, display a coherent and weak variability throughout the core, with a visible rise in the uppermost 0–10-cm layer, where TOC was slightly increased. In core AMK-5194, the Mn/Fe ratio, used as redox condition proxy, displayed of few peaks: at depths of 10 cm, indicating the upper oxidized layer, as well as at depths of 115 cm and 290 cm. The latter depths are recognized as the boundary between Late/Mid Holocene and Early Holocene/Late Deglaciation periods, respectively. In that time, the speed of bottom currents rose, which led to an enlargement of oxygen concentration in water. It should be noticed that, down the core, the Mn/Fe ratios exhibit an opposite trend to that of Si/Al, Ti/Al, and Fe/Al, which evidently supports an application of these ratios for identification of contrast geochemical characteristics of sedimentation paleo-environment.

(5) Data on elemental distribution in both the recent sediments of the Kola Transect and cores from Central Deep, Bear Island Trough, Cambridge Strait, and Russkaya Gavan' Bay, indicate their noticeable dependence on change in the grain size composition, which in turn is related to bottom topography and

hydrodynamics conditions. A contrasting behavior of different elements was revealed: Si, Zr, and Ba display a coherent distribution pattern with the coarse-grained fraction, while Ca and Mn proved to be the most sensitive elements to change in proportion of silt and clay fractions correspondingly.

(6) The presented data on the potentially toxic heavy metals, such as Pb, Cu, and Zn in recent surface sediments of the central part of the basin, suggest a rather weak additional contribution of sedimentary matter of anthropogenic origin. The exception is As, whose average content (19 ppm) exceeds the UCC values (8 ppm); however, there are no published data on the regional As background values.

(7) In recent sediments of the Central Deep (AMK-5193) with increased contents of clay minerals, mostly illite, analysis of geochemical speciation Al and heavy metals yielded a strong predominance of lithogenic fraction for Al, Fe, and Cr in their accumulation. In the oxic-suboxic conditions of the upper layers, where the content of TOC is elevated and the early diagenetic fractionation occurs, the redox-sensitive Mn and Mo are predominantly accumulated in the exchangeable (adsorbed on clay minerals/bound to carbonates) fraction. The presented data indicate that early diagenetic fractionation of metals, such as Cu, Mn, Mo, Ni, and Pb, took place in oxic-suboxic conditions. The accumulation of heavy metals, such as Cu, Pb, Co, Ni, Mn, and Mo in sediments, is attributed to adsorption and immobilization processes. Among the rest of metals, Cu exhibited the larger proportion bound to organic matter. A similar type of the Mn and other metals' partitioning in the surface sediments might promote the formation of the Mn-nodules and concretions, which were found on the Arctic seafloor and described in [98–100]. Those Fe-Mn-hydroxide concretions differ strongly in reduced Mn, Fe, and trace metal contents from the deep-sea nodules of the Pacific due to a specific Arctic sedimentation environments.

(8) In the unconsolidated uppermost surface sediments of the Cambridge Strait, the Franz Josef Land Archipelago, new mineral forms are generated during early diagenesis. The diffraction characteristics of registered zeolites (Mordenite, Ca-Heulandite, and Clinoptilolite) correspond to the Ca-forms of these minerals. It means that the structural positions of freely bound cations are mainly filled with the  $\text{Ca}^{2+}$  cations supplied to the bottom waters as a result of basalt epigenesis. The genesis of the diagnosed zeolites has not been studied in detail. The appearance of these phases can be the result of hydrogenic precipitation from bottom waters, galmirolysis, as a result of interaction of the sediment solid phase with bottom water, as well as mineral formation can occur inside the sediment when it interacts with pore waters.

**Supplementary Materials:** The following are available online at <http://www.mdpi.com/2075-163X/10/7/593/s1>, Table S1: Grain size data of sediment core AMK-5194; Table S2: Grain-size data of cores AMK-5424, -5432, -5454; Table S3: Specific radioactivity of radionuclides in sediment core 5454. Data for  $^{137}\text{Cs}$  and excess  $^{210}\text{Pb}$  are given for sampling date; Table S4: Specific radioactivity of radionuclides in sediment core 5432; Table S5: Specific radioactivity of radionuclides in sediment core 5424; Table S6: XRF data for MUC cores AMK-5424, -5432, -5454; Table S7: XRF data for sediments at Kola Transect; Table S8: XRF data of sediment GC AMK-5194; Table S9: Correlation matrix of surface sediment; Table S10. Distribution of Al, Fe, Mn and trace metals' geochemical fractions in the AMK-5193 core, the Central Deep of the Barents Sea.

**Author Contributions:** Project idea: L.L.D.; Sampling and on board preparation: N.P., D.B.; Lithological discription: N.P., E.N.; Grain size analysis and data interpretation: T.A., N.P.; XRD analysis and interpretation: O.D.; Radionuclide analysis and interpretation: R.A.; Chemical analysis and data processing: D.B.; XRF analysis: A.S., A.B.; Writing: L.L.D., O.D., R.A., T.A., E.N., N.P.; Funding acquisition: L.L.D. All authors have read and agreed to the published version of the manuscript.

**Funding:** This research was carried out in the framework a State Assignment of Ministry of Science and High Education, Russia (program no. 0149-2019-0007); field data were obtained in cruises supported by the Russian Science Foundation (<https://www.rscf.ru>), project no. 14-50-00095, "Interaction of Geospheres and Mineral Resources of the World Ocean", led by Academician A.P. Lisitsyn; interpretation of data and preparation of manuscript was supported by the Russian Science Foundation (<https://www.rscf.ru>), project no. 19-17-00234, led by I. Nemirovskaya. This work was supported in part (gamma spectroscopy of 5424 core) by Lomonosov Moscow State University Program of Development.

**Acknowledgments:** We are grateful to Academician RAS, Alexander P. Lisitzin (Shirshov Institute of Oceanology RAS (IO RAS), Moscow, Russia), for initiation of the Arctic investigations over 25 years ago and for supporting this research. The authors are grateful to Marina Kravchishina (IO RAS) for lithological description of cores, Nina Kozina (IO RAS) for lithology description of the AMK-5424, -5432, and -5454 cores, Igor Proshin and Elena

Zakharova (IPCE RAS), for their assistance in performing gamma-ray spectrometry, and to Natalia Kuzmenkova (MSU) for providing reference materials.

**Conflicts of Interest:** The authors declare no conflict of interest.

## References

1. Lubinski, D.J.; Polyak, L.; Forman, S.L. Freshwater and Atlantic water inflows to the deep northern Barents and Kara seas since ca 13 14C ka: Foraminifera and stable isotopes. *Quat. Sci. Rev.* **2001**, *20*, 1851–1879. [\[CrossRef\]](#)
2. Ivanova, E.; Murdmaa, I.; Duplessy, J.-C.; Paterne, M. Late Weichselian to Holocene paleoenvironments in the Barents Sea. *Glob. Planet. Chang.* **2002**, *34*, 209–218. [\[CrossRef\]](#)
3. Murdmaa, I.O.; Ivanova, E.V. Postglacial sedimentation history in shelf depressions of the Barents Sea. *Lithol. Miner. Resour.* **1999**, *6*, 576–595.
4. Murdmaa, I.; Ivanova, E.; Duplessy, J.-C.; Levitan, M.; Khusid, T.; Bourtmann, M.; Alekhina, G.; Alekseeva, T.; Belousov, M.; Serova, V. Facies system of the central and Eastern Barents Sea since the last glaciation to present. *Mar. Geol.* **2006**, *230*, 275–303. [\[CrossRef\]](#)
5. Gurvich, E.G.; Vlasova, I.E.; Gordeev, V.Y.; Isaeva, A.B. Chemical composition of bottom sediments of the Barents Sea. In *Experience of System Oceanologic Studies in the Arctic*; Lisitsyn, A.P., Vinogradov, M.E., Romankevich, E.A., Eds.; Science World: Moscow, Russia, 2001; pp. 616–635, (In Russian, with English Abstr.).
6. Chase, Z.; Ellwood, M.J.; Van de Flierdt, T. Discovering the Ocean's Past through Geochemistry. *Elements* **2018**, *14*, 397–402. [\[CrossRef\]](#)
7. Calvert, S.E.; Pedersen, T.F. Elemental proxies for palaeoclimatic and palaeoceanographic variability in marine sediments: Interpretation and application. In *Developments in Marine Geology, Proxies in Late Cenozoic Paleoceanography*; Hillaire-Marcel, C., De Vernal, A., Eds.; Elsevier: Amsterdam, The Netherlands, 2007; pp. 568–644.
8. Spofforth, D.J.A.; Pälike, H.; Green, D.R.H. Paleogene record of elemental concentrations in sediments from the Arctic Ocean obtained by XRF analyses. *Paleoceanography* **2008**, *3*, PA1S09. [\[CrossRef\]](#)
9. Polyak, L.; Bischof, J.; Ortiz, J.D.; Darby, D.A.; Channell, J.E.T.; Xuand, C.; Kaufman, D.S.; Løvlie, R.; Schneider, D.A.; Eberl, D.D.; et al. Late quaternary stratigraphy and sedimentation patterns in the western Arctic Ocean. *Glob. Planet. Chang.* **2009**, *68*, 5–17. [\[CrossRef\]](#)
10. Jonkers, L.; Moros, M.; Prince, M.A.; Dokken, T.; Anderssen Dahl, K.; Dijkstra, N.; Perner, K.; Brummer, G.-J.A. A reconstruction of sea surface warming in the North Atlantic during MIS 3 ice-rafting events. *Quat. Sci. Rev.* **2012**, *29*, 1791–1800. [\[CrossRef\]](#)
11. Krylov, A.A. The Clay minerals as indicators of Late-Quaternary sedimentation conditions in the area of the Mendeleev Ridge. *Lithol. Miner. Resour.* **2013**, *6*, 507–518.
12. Schoster, F.; Behrends, M.; Muller, C.; Stein, R.; Wahsner, M. Modern river discharge and pathways of supplied material in the Eurasian Arctic Ocean: Evidence from mineral assemblages and major and minor element distribution. *Int. J. Earth Sci.* **2000**, *89*, 486–495. [\[CrossRef\]](#)
13. Maslov, A.V.; Kuznetsov, A.B.; Politova, N.V.; Kozina, N.V.; Novigatsky, A.N.; Schevchenko, V.P. The isotope composition of Nd, Pb and Sr in modern bottom sediments of the Barents Sea. *Dokl. Earth Sci.* **2019**, *485*, 71–75. [\[CrossRef\]](#)
14. Gurevich, V.I. *The Modern Sedimentation and Geologic Ecology of the Western Arctic Eurasian Shelf*; Science World: Moscow, Russia, 2002; p. 135. (In Russian)
15. Romankevich, E.A.; Danyushevskaya, A.I.; Belyaeva, A.N.; Rusanov, V.P. *Biogeochemistry of Organic Matter in the Arctic Seas*; Nauka: Moscow, Russia, 1982; p. 256. (In Russian)
16. Gurevich, V.I. *Recent Sedimentogenesis and Environment on the Arctic Shelf of Western Eurasia*; Norsk Polar Inst.: Oslo, Norway, 1995; Volume Voulme 13, p. 92.
17. Nurnberg, D. Biogenic barium and opal in shallow Eurasian shelf sediments in relation to the pelagic Arctic Ocean environment. In *Surface Sediment Composition and Sedimentary Processes in Central Arctic Ocean and along the Eurasian Continental Margin*; AWI: Bremerhaven, Germany, 1996; pp. 96–118.

18. Bogdanov, Y.A.; Murdmaa, I.O.; Gurvich, E.G.; Pimenov, N.Y.; Pavlova, G.A.; Karpenko, A.A.; Vlasova, I.E.; Plishkin, A.N. The study of upper part of Barents Sea sedimentary layer for sedimentation history outline and paleoceanographic reconstructions. In *Experience of System Oceanologic Studies in the Arctic*; Lisitsyn, A.P., Vinogradov, M.E., Romankevich, E.A., Eds.; Science World: Moscow, Russia, 2001; pp. 598–615. (In Russian).
19. Strekopytov, S.V. The iron and sulfur occurrence forms in bottom sediments of the Barents Sea. In *Experience of System Oceanologic Studies in the Arctic*; Lisitsyn, A.P., Vinogradov, M.E., Romankevich, E.A., Eds.; Science World: Moscow, Russia, 2001; pp. 586–597.
20. Ivanov, G.I. *Geology and Ecology of the Western Arctic Shelf of Russia: Lithological and Geochemical Aspects*; Kamensky, A.N.A., Ed.; Nauka: Saint Petersburg, Russia, 2006; p. 303.
21. Novikov, M.A.; Zhilin, A.Y. Distribution type of heavy metals in bottom sediments of the Barents Sea (based on statistical analysis). *Vestnik KRAUNZ. Earth Sci.* **2016**, *1*, 78–88.
22. Poulton, S.W.; Raiswell, R. The low-temperature geochemical cycle of iron: From continental fluxes to marine sediment deposition. *Am. J. Sci.* **2002**, *302*, 774–805. [[CrossRef](#)]
23. Raiswell, R.; Canfield, D.E. The iron biogeochemical cycle: Past and present. *Geochem. Perspect. Lett.* **2012**, *1*, 1–2. [[CrossRef](#)]
24. Demina, L.L.; Levitan, M.A.; Politova, N.V. Speciation of some heavy metals in bottom sediments of the Ob and Yenisei estuarine zones. *Geochem. Int.* **2006**, *44*, 182–195. [[CrossRef](#)]
25. Demina, L.L.; Bud'ko, D.F.; Alekseeva, T.N.; Novigatsky, A.N.; Filippov, A.S.; Kochenkova, A.I. Partitioning of trace elements in the process of early diagenesis of bottom sediments in the White Sea. *Geochem. Int.* **2017**, *55*, 144–149. [[CrossRef](#)]
26. Koukina, S.E.; Vetrov, A.A. Metal forms in sediments from Arctic coastal environments in Kandalaksha Bay, White Sea, under separation processes. *Estuar. Coast. Shelf Sci.* **2013**, *130*, 21–29. [[CrossRef](#)]
27. Grotti, M.; Soggia, F.; Ianni, C.; Magi, E.; Udisti, R. Bioavailability of trace elements in surface sediments from Kongsfjorden, Svalbard. *Mar. Pollut. Bull.* **2013**, *77*, 367–374. [[CrossRef](#)] [[PubMed](#)]
28. Budko, D.F.; Demina, L.L.; Lisitzin, A.P.; Kravchishina, M.D.; Politova, N.V. Occurrence forms of trace metals in recent bottom sediments from the White and Barents Seas. *Dokl. Earth Sci.* **2017**, *474*, 552–556. [[CrossRef](#)]
29. Budko, D.F.; Demina, L.L.; Novichkova, E.A.; Polyakova, Y.I.; Kravchishina, M.D.; Melenevsky, V.N. Postglacial sedimentation in the White Sea (Northwestern Russia) reconstructed by integrated microfossils' and geochemical data. *Quat. Res.* **2020**, *93*, 110–123. [[CrossRef](#)]
30. Vasiliev, V.V.; Viskunova, K.G.; Kiiko, O.A.; Kozlov, S.A.; Kostin, D.A.; Lopatin, B.G.; Markina, N.V.; Orgo, V.V.; Pavlov, S.P.; Penedyuk, E.V.; et al. *State geological map of the Russian Federation. Scale 1:1,000,000*, 3rd ed.; Northern-Kara-Barents Seas. L T-41–44—Cape Zhelaniya; Kartfabrika VSEGEI: Saint Petersburg, Russia, 2013; p. 200. (In Russian)
31. Vorren, T.O.; Laberg, J.S. Late glacial air temperature, oceanographic and ice sheet interactions in the southern Barents Sea region. In *Late Quaternary Paleocanography of the North Atlantic Margins*; Andrews, J.T., Austin, W.E., Bergsten, W.E.N., Jennings, A.E., Eds.; Geological Society Special Publications: London, UK, 1996; Volume 111, pp. 303–321.
32. Thiede, J.; Mangerud, J. New Map Revises Extent of Last Ice Sheet Over Barents and Kara Seas. *EOS Trans.* **1999**, *80*, 493–494. [[CrossRef](#)]
33. Polyak, L.; Gataullin, V.; Okuneva, O.; Stelle, V. New constrains on the limits of the Barents-Kara ice sheet during the Last Glacial Maximum based on borehole stratigraphy from the Pechora Sea. *Geology* **2000**, *28*, 611–614. [[CrossRef](#)]
34. Svendsen, J.I.; Gataullin, V.; Mangerud, J.; Poljak, L. The glacial history of the Barents and Kara Sea region. In *Quaternary Glaciations—Extent and Chronology*; Ehlers, J., Gibbard, P., Eds.; Elsevier: Amsterdam, The Netherlands, 2004; Volume 1, pp. 369–378.
35. Barash, M.S. *Quaternary Paleocanology of the Atlantic Ocean*; Nauka: Moscow, Russia, 1988; p. 254. (In Russian)
36. Ivanova, E.V.; Duplessy, J.C.; Paterne, M.; Murdmaa, I.O.; Levitan, M.A.; Vetrov, A.A.; Romankevich, E.A.; Khusid, T.A. *The Influence of Climate and Thermohaline Circulation on the Productivity of the Eastern Barents Sea during the Holocene*; ICP VII Program and Abstracts: Sapporo, Japan, 2001; p. 125.
37. Murdmaa, I.O.; Polyak, L.; Ivanova, E.V.; Khromova, N.V. Paleoenvironments in the Russkaya Gavan' Fjord (NW Novaya Zemlya) during the Last Millenium. *Palaeogeogr. Palaeoclimatol. Palaeoecol.* **2004**, *209*, 141–154. [[CrossRef](#)]



38. Hald, M.; Kolstad, V.; Polyak, L.; Forman, S.L.; Herlihy, F.A.; Ivanov, G.; Nescheretov, A. Late glacial and Holocene paleoceanography and sedimentary environments in the Saint Anna Trough, Eurasian Arctic Ocean margin. *Palaeogeogr. Palaeoclim. Palaeoecol.* **1999**, *146*, 229–249. [CrossRef]
39. Polyak, L.; Mikhailov, V. Post-glacial environments of the southeastern Barents Sea: Foraminiferal evidence. In *Late Quaternary Paleoceanography of the North Atlantic Margins*; Andrews, J.T., Austin, W.E.N., Bergsten, H., Jennings, A.E., Eds.; Geological Society Special Publications: London, UK, 1996; Volume 111, pp. 323–337.
40. Elverhoi, A.; Pfirman, S.L.; Solheim, A.; Larsen, B.B. Glaciomarine sedimentation in epicontinental seas exemplified by the Northern Barents Sea. *Mar. Geol.* **1989**, *85*, 225–250. [CrossRef]
41. Aybulatov, N.M.; Matyushenko, V.A.; Shevchenko, V.P.; Politova, N.V. New data on structure of lateral suspended matter fluxes in the periphery of the Barents Sea. *Geoecology* **1999**, *6*, 526–540.
42. Lisitzin, A.P. *Sea-Ice and Iceberg Sedimentation in the World Ocean: Present and Past*; Springer: Berlin, Germany, 2002; p. 563.
43. AMAP Assessment 2007: Oil and Gas Activities in the Arctic—Effects and Potential Effects. Arctic Monitoring and Assessment Programme. V.1. Published by: AMAP. 2010. Available online: <http://www.amap.no/documents/download/1015> (accessed on 1 June 2010).
44. Pavlidis, Y.A.; Polyakova, E.I. Late Pleistocene and Holocene depositional environments and paleoceanography of the Barents Sea: Evidence from seismic and biostratigraphic data. *Mar. Geol.* **1997**, *143*, 189–205. [CrossRef]
45. Shevchenko, V.P. The influence of aerosols on the oceanic sedimentation and environmental conditions in the Arctic. *Ber. Polar Meeresforsch (Rep. Polar Mar. Res.)* **2003**, *464*, 153.
46. Djenynk, S.L. Non-periodical and summarized currents. In *Hydrometeorology and Hydrochemistry of USSR. 1. Barents Sea*; Issue 1. Hydrologic Meteorologic Conditions; Gidrometizdat: Leningrad, Russia, 1990; pp. 33–40. (In Russian)
47. Byshev, V.I.; Galerkin, L.I.; Gorotov, A.S. Thermohaline structure of the Barents Sea waters in September 1998. In *Experience of System Oceanologic Studies in the Arctic*; Lisitzin, A.P., Vinogradov, M.E., Romankevich, E.A., Eds.; Science World: Moscow, Russia, 2001; pp. 102–109. (In Russian).
48. Zubakin, G.K. Sea-ice conditions and location of the ice margin. In *Hydrometeorology and Hydrochemistry of USSR. 1. Barents Sea*; Issue 1. Hydrometeorological Conditions; Gidrometizdat: Leningrad, Russia, 1990; pp. 250–254. (In Russian)
49. Wassmann, P.; Slagstad, D. Annual dynamics of carbon flux in the Barents Sea: Preliminary results. *Norsk Geol. Tidsskr.* **1991**, *71*, 231–234.
50. Romankevich, E.A.; Vetrov, A.A. *The Carbon Cycle in Russian the Arctic Seas*; Nauka: Moscow, Russia, 2001; p. 302.
51. Lisitzin, A.P.; Demina, L.L. Introduction. In *Sedimentation Processes in the White Sea: The White Sea Environment Part II*; Lisitsyn, A.P., Demina, L.L., Eds.; Handbook of Environmental Chemistry; Springer-Nature: Berlin, Germany, 2018; Volume 82, pp. 1–12. [CrossRef]
52. Politova, N.V.; Novigatsky, A.N.; Kozina, N.V.; Terpugova, S.A. Multidisciplinary research in the Barents Sea on cruise 67 of the R/V Akademik Mstislav Keldysh. *Oceanology* **2018**, *58*, 499–501. [CrossRef]
53. Kravchishina, M.D.; Novigatskii, A.N.; Savvichev, A.S.; Pautova, L.A.; Lisitsyn, A.P. Studies on sedimentary systems in the Barents Sea and Norwegian–Greenland basin during cruise 68 of the R/V Akademik Mstislav Keldysh. *Oceanology* **2019**, *59*, 158–160. [CrossRef]
54. Petelin, V.P. *Granulometrical Analysis of Marine Sediments*; Nauka: Moscow, Russia, 1967; p. 218. (In Russian)
55. Bezrukov, P.L.; Lisitzyn, A.P. Classification of bottom sediments in modern basins. *Proceed. Inst. Oceanol. USSR Acad. Sci.* **1960**, *32*, 179.
56. Ure, A.M.; Quevauviller, P.; Muntau, H.; Griepink, B. Speciation of heavy metals in soils and sediments. An account of the improvement and harmonization of extraction techniques undertaken under the auspices of the BCR of the Commission of the European Community. *Int. J. Environ. Anal. Chem.* **1993**, *51*, 135–151. [CrossRef]
57. Luoma, S.N.; Bryan, G.W. A statistical assessment of the forms of trace metals in oxidized estuarine sediments employing chemical extractants. *Sci. Total Environ.* **1981**, *17*, 165–196. [CrossRef]
58. Chester, R.; Hughes, M.J. A chemical technique for separation of ferromanganese minerals and adsorbed trace metals from pelagic sediments. *Chem. Geol.* **1967**, *3*, 249–262. [CrossRef]
59. Kitano, Y.; Fujiyoshi, R. Selective chemical leaching of Cd, Cu, Mn and Fe in marine sediments. *Geochem. J.* **1980**, *14*, 122–128. [CrossRef]

60. Quevauviller, P.; Ure, A.; Muntau, H.; Griepink, B. Improvement of analytical measurements within the BCR programme: Single and sequential extraction procedures applied to soil and sediment analysis. *Int. J. Environ. Anal. Chem.* **1993**, *51*, 129–134. [\[CrossRef\]](#)
61. Pueyo, M.; Rauret, G.; Luck, D. Certification of the extractable contents of Cd, Cr, Cu, Ni, Pb and Zn in a freshwater sediment following a collaboratively tested and optimized three-step sequential extraction procedure. *J. Environ. Monit.* **2001**, *3*, 243–250. [\[CrossRef\]](#)
62. Sutherland, R.A.; Tack, F.M.G. Fractionation of Cu, Pb and Zn in certified reference soils SRM 2710 and SRM 2711 using the optimized BCR sequential. *Adv. Environ. Res.* **2003**, *8*, 37–50. [\[CrossRef\]](#)
63. Moore, D.M.; Reynolds, R.C. *X-ray Diffraction and the Identification and Analysis of Clay Minerals*, 2nd ed.; Oxford university Press: Oxford, UK; New York, NY, USA, 1997; p. 378.
64. Frank-Kamenetsky, V.A. (Ed.) *X-ray Analysis of the Main Types of Rock-Forming Minerals*; Nedra: Leningrad, Russia, 1983; p. 360. (In Russian)
65. Krishnaswamy, S.; Lal, D.; Martin, J.M.; Meybeck, M. Geochronology of lake sediments. *Earth Planet. Sci. Lett.* **1971**, *11*, 407–414. [\[CrossRef\]](#)
66. Robbins, J.A.; Edgington, D.N. Determination of recent sedimentation rates in Lake Michigan using Pb-210 and Cs-137. *Geochim. Cosmochim. Acta* **1975**, *39*, 285–304. [\[CrossRef\]](#)
67. Wedepohl, H. The composition of the continental crust. *Geochim. Cosmochim. Acta* **1995**, *59*, 1217–1239. [\[CrossRef\]](#)
68. Moros, M.; Kuijpers, A.; Snowball, I.; Lassen, S.; Backstrom, D.; Ginge, P.; McManus, J. Were glacial iceberg surges in the North Atlantic triggered by climatic warming? *Mar. Geol.* **2002**, *192*, 393–417. [\[CrossRef\]](#)
69. Erbs-Hansen, D.R.; Knudsen, K.L.; Olsen, J.; Lykke-Andersen, H.; Underbjerg, J.A.; Sha, L. Paleooceanographic development of Sisimiut, West Greenland, during the mid- and late Holocene: A multiproxy study. *Mar. Micropaleontol.* **2013**, *102*, 79–97. [\[CrossRef\]](#)
70. Romankevich, E.A.; Vetrov, A.A.; Vinogradov, M.E.; Vedernikov, V.I. Some Elements of the Carbon Cycle in the Russian Arctic Seas. Fluxes of Carbon from Land, Carbon in Bottom Sediments, Elements of Budget. *Oceanology* **2000**, *40*, 363–372.
71. Sayago-Gil, M.; López-González, N.; Long, D.; Fernández-Salas, L.M.; Durán-Muñoz, P. Multi-proxy approach for identifying Heinrich Events in sediment cores from Hatton Bank (NE Atlantic Ocean). *Geosciences* **2020**, *10*, 14. [\[CrossRef\]](#)
72. Migdisov, A.A. The ratio of titanium and aluminum in sedimentary rocks. *Geochem. Int.* **1960**, *2*, 149–163.
73. Demina, L.; Novichkova, E.; Lisitzin, A.; Kozina, N. Geochemical signatures of paleoclimate changes in the sediment cores from the Gloria and Snorri Drifts (Northwest Atlantic) over the Holocene-Mid Pleistocene. *Geosciences* **2019**, *9*, 432. [\[CrossRef\]](#)
74. Jakobsson, M.; Løvlie, R.; Al-Hanbali, H.; Arnold, E.; Backman, J.; Mörrh, M. Manganese and color cycles in Arctic Ocean sediments constrain Pleistocene chronology. *Geology* **2000**, *28*, 23–26. [\[CrossRef\]](#)
75. Chester, R. *Marine Geochemistry*; Blackwell: London, UK, 2000; p. 506.
76. Tribouillard, N.; Algeo, T.J.; Lyons, T.; Ribouleau, A. Trace metals as paleoredox and paleoproductivity proxies: An update. *Chem. Geol.* **2006**, *232*, 12–32. [\[CrossRef\]](#)
77. Naeher, S.; Gilli, A.; North, R.P.; Hamann, Y.; Schubert, C.J. Tracing bottom water oxygenation with sedimentary Mn/Fe ratios in Lake Zurich, Switzerland. *Chem. Geol.* **2013**, *352*, 125–133. [\[CrossRef\]](#)
78. Zaborska, A.; Carroll, J.; Papucci, C.; Torricelli, L.; Carroll, M.L.; Walkusz-Miotk, J.; Pempkowiak, J. Recent sediment accumulation rates for the Western margin of the Barents Sea. *Deep Sea Res. Part II Top. Stud. Oceanogr.* **2008**, *55*, 2352–2360. [\[CrossRef\]](#)
79. Lisitzin, A.P. Sedimentation in the World Ocean. International Society of Ecology, Paleooceanology and Mineralogy. *Spec. Publ.* **1972**, *17*, 218.
80. Lisitsyn, A.P. The up-to-date insights to sediment formation in marine basins: An ocean as a natural recorder of the Earth geospheres' interaction. In *The World Ocean*; v. 2; Nigmatulin, R.I., Lobkovskii, L.I., Eds.; Science World: Moscow, Russia, 2015; pp. 331–553. (In Russian)
81. Bakke, T.; Breedveld, G.; Kællgvist, T. *Veileder for Klassifisering av Miljøkvalitet i Fjorder og Kystfarvann—Revisjon av Lassifisering av Metaller og Organiske Miljøgifter i van nog Sedimenter*; SFT Veiledning: Oslo, Norway, 2007; p. 12. (In Norwegian)

82. Maslov, A.V.; Kozina, N.V.; Politova, N.V.; Shevchenko, V.P. About analysis of distribution of a number of trace and rare elements in modern bottom sediments of the Barents sea (based on data of 67 cruise R/V “Akademik Mstislav Keldysh”. Annual Report-2017. *Proc. Inst. Geol. Ural Branch RAS* **2018**, *165*, 53–59.
83. Imai, N.; Ando, A.; Takeda, E. Minor elements in Japanese coal (II). *Bull. Geol. Surv. Jpn.* **1984**, *35*, 287–314.
84. Yudovich, Y.E.; Ketris, M.P. Arsenic in coal: A review. *Int. J. Coal Geol.* **2005**, *61*, 141–196. [[CrossRef](#)]
85. Ohta, A.; Imai, N.; Terashima, S.; Tachibana, Y.; Ikehara, K.; Katayama, H.; Noda, A. Factors controlling regional spatial distribution of 53 elements in coastal sea sediments in northern Japan: Comparison of geochemical data derived from stream and marine sediments. *Appl. Geochem.* **2010**, *25*, 357–376. [[CrossRef](#)]
86. Bergan, T.D. Radioactive fallout in Norway from atmospheric nuclear weapons tests. *J. Environ. Radioact.* **2002**, *60*, 189–208. [[CrossRef](#)]
87. Unscear 2000 Report, Vol. I: Sources and Effects of Ionizing Radiation. United Nations Scientific Committee on the Effects of Atomic Radiation UNSCEAR 2000 Report to the General Assembly, with Scientific Annexes United Nations, NY. 2000. Available online: [http://www.unscear.org/unscear/en/publications/2000\\_1.html](http://www.unscear.org/unscear/en/publications/2000_1.html) (accessed on 1 May 2016).
88. Gray, J.; Jones, S.R.; Smith, A.D. Discharges to the environment from the Sellafield Site, 1951–1992. *J. Radiol. Prot.* **1995**, *15*, 99–131. [[CrossRef](#)]
89. Kershaw, P.; Baxter, A. The transfer of reprocessing wastes from north-west Europe to the Arctic. *Deep Sea Res. Part II Top. Stud. Oceanogr.* **1995**, *42*, 1413–1448. [[CrossRef](#)]
90. Brown, J.E.; Iospje, M.; Kolstad, K.E.; Lind, B.; Rudjord, A.L.; Strand, P. Temporal trends for <sup>99</sup>Tc in Norwegian coastal environments and spatial distribution in the Barents Sea. *J. Environ. Radioact.* **2002**, *60*, 49–60. [[CrossRef](#)]
91. Orlandini, K.A.; Penrose, W.R.; Nelson, D.M. Pu(V) as the stable form of oxidized plutonium in natural waters. *Mar. Chem.* **1986**, *18*, 49–57. [[CrossRef](#)]
92. Sanchez, A.L.; Gastaud, J.; Noshkin, V.; Buesseler, K.O. Plutonium oxidation states in the southwestern Black Sea: Evidence regarding the origin of the cold intermediate layer. *Deep Sea Res. Part A. Oceanogr. Res. Pap.* **1991**, *38*, S845–S853. [[CrossRef](#)]
93. Zaborska, A.; Mielinski, J.W.; Carroll, J.; Papucci, C.; Pempkowiak, J. Sources and distributions of <sup>137</sup>Cs, <sup>238</sup>Pu, <sup>239</sup>,<sup>240</sup>Pu radionuclides in the north-western Barents Sea. *J. Environ. Radioact.* **2010**, *101*, 323–331. [[CrossRef](#)]
94. Aarkrog, A. Radioactivity in polar regions—Main sources. *J. Environ. Radioact.* **1994**, *25*, 21–35. [[CrossRef](#)]
95. Leppänen, A.-P.; Kasatkina, N.; Vaaramaa, K.; Matishov, G.G.; Solatie, D. Selected anthropogenic and natural radioisotopes in the Barents Sea and off the western coast of Svalbard. *J. Environ. Radioact.* **2013**, *126*, 196–208. [[CrossRef](#)]
96. Gwynn, J.P.; Heldal, H.E.; Gåfvert, T.; Blinova, O.; Eriksson, M.; Sværen, I.; Brungot, A.L.; Strålberg, E.; Møller, B.; Rudjord, A.L. Radiological status of the marine environment in the Barents Sea. *J. Environ. Radioact.* **2012**, *113*, 155–162. [[CrossRef](#)]
97. Matishov, G.G.; Matishov, D.G.; Solatie, D.; Kasatkina, N.E.; Leppanen, A. Natural decrease of the intensity level of artificial radioactive isotopes in the Barents Sea. *Dokl. Earth Sci.* **2009**, *427*, 1006–1011. [[CrossRef](#)]
98. Bogdanov, A.Y.; Gorshkov, A.I.; Gurvich, E.G. Ferromanganese nodules of the Kara Sea. *Oceanology* **1994**, *34*, 789–800.
99. Baturin, G.N. Variations in the composition of ferromanganese nodules in the Kara Sea. *Oceanology* **2011**, *51*, 153–161. [[CrossRef](#)]
100. Baturin, G.N.; Dubinchuk, V.T. On the composition of ferromanganese nodules of the Chukotka and East Siberian Seas. *Dokl. Earth. Sci.* **2011**, *440*, 93–99. [[CrossRef](#)]

